VILNIUS UNIVERSITY
CENTER FOR PHYSICAL SCIENCES AND TECHNOLOGY

MAKSIM IVANOV

GRAIN SIZE EFFECT ON DIELECTRIC PROPERTIES OF FERROELECTRICS AND RELAXORS

Doctoral dissertation
Technological Sciences, Material Engineering (08T)

Vilnius, 2014

The dissertation was prepared in Vilnius university in 2010 – 2014.

Scientific supervisor:

prof. habil. dr. Jūras Banys (Vilnius university, Physical sciences, Physics 02P).

Acknowledgments

The author is sincerely grateful to:

the scientific supervisor prof. habil. dr. Jūras Banys for supervision and help in achieving the goal of getting results and writing the thesis along with other nice things and perks in the lab;

dr. Robertas Grigalaitis for advices, help and collaboration throughout the years in the lab;

dr. Jan Macutkevič and students Sergejus Balčiūnas and Ringailė Marija Katiliūtė for collaboration with experimental work and writing papers;

other colleagues of the lab (in no particular order): Šarūnas Bagdzevičius, Džiugas Jablonskas, Šarūnas Svirskas, Ieva Kranauskaitė, Rūta Mackevičiūtė, Edita Palaimienė, Aurimas Sakanas, Jaroslavas Belovickis, prof. Vytautas Samulionis, Maksimas Anbinderis, Dainius Gabrielaitis, Ilona Zamaraitė, Kęstutis Bučinskas, Mantas Šimėnas, dr. Saulius Rudys and others – for collaboration in various projects, help with experiments, support in need, friendly atmosphere in and outside the lab and other important experiences;

prof. J.-M. Kiat, prof. M. Alguero and dr. A. Stanulis for providing superb samples for investigations;

all employees of the Faculty of Physics and Department of Radiophysics in particular for collaboration and help;

my family members for support.

Table of Contents

1. Introduction

Ferroelectrics are materials that exhibit spontaneous polarization, which can be switched by external electric field. Ferroelectrics and related materials (such as ferroelectric relaxors) are a widely investigated class of materials due to both scientific and engineering interest, with the interests often deeply entangled. From scientific point of view, ferroelectric materials are easy to understand only in case of the most simple models – in the absence of defects, chemical disorder, other dielectric anomalies or (competing) order parameters.. However, there is a variety of different phenomena taking place in both bulk and nanoscale materials. Formation of domain walls, stresses, interface effects are just a few of the most interesting topics.

Engineers are often taking advantage of memory effects and other properties. Switchable spontaneous polarization is used to produce memory cells (i.e. FeRAMs), high dielectric constant is important for production of electric capacitors, all ferroelectrics are also pyro- and piezoelectrics. This allows to use them as sensors, actuators, energy harvesters and in many other applications. Photovoltaic effect also becomes very important in the recent years.

It is important to realise, that modern technologies are driven towards miniaturisation of devices. Thus it becomes highly important to understand how properties of ferroelectric materials change at the nanoscale. Understanding of underlying phenomena is very untrivial. It is clear, that surfaces play a major role. Firstly, properties of the surface are very different from the bulk. Secondly, surface is a defect, which influences the bulk through pinning of ferroelectric domains walls. Mechanical strain at the surface is another highly important factor. There are other phenomena influencing the resulting properties in highly non-linear, and sometimes hardly predictable, ways. Research of size effects on properties of ferroelectric materials is very important for both scientists and engineers.

1.1. Aim and tasks of the work

Main aim of the current work is to understand how reduction of grain size changes dielectric properties of dense ferroelectric and relaxor ceramics and compare the latter with size effect in a powdered relaxor.

Tasks of the current work are:

1. Investigate grain size effect in powders of a canonical ferroelectric relaxor $PbMg_{⅓}Nb_{⅔}O_3$ (PMN) and compare it with PMN ceramics.
2. Investigate grain size effect in dense ceramics of a relaxor with a spontaneous phase transition $PbSc_{½}Nb_{½}O_3$ (PSN) and compare it with PMN.
3. Investigate and model grain size effect in dense ceramics of a ferroelectric $0.36BiScO_3$-$0.64PbTiO_3$ (BSPT) and compare it with other ferroelectrics and relaxors.
4. Investigate ceramics of Ba_2SnO_4 in search of dielectric anomalies and compare the result with similar investigations of $BaSnO_3$.

In all cases investigation was meant to be performed by means of broadband dielectric spectroscopy.

1.2. Scientific novelty

1. For the first time powders of a canonical ferroelectric relaxor $PbMg_{⅓}Nb_{⅔}O_3$ (PMN) with grain size ranging from 15 nm to 1 μm were investigated in 20 Hz – 1 MHz frequency and 100 – 300 K temperature ranges. It was found that interactions of polar nanoregions across grain boundaries must take place in dense ceramics.
2. For the first time dense ceramics of a relaxor with spontaneous phase transition $PbSc_{½}Nb_{½}O_3$ (PSN) with grain size ranging from 20 nm to 80 nm were investigated in 20 Hz – 40 GHz frequency and 100 K – 500 K temperature ranges. It was found that dielectric anomaly is suppressed

upon decrease of grain size, although phase transition does not vanish.

3. For the first time dense ceramics of a ferroelectric $0.36BiScO_3$-$0.64PbTiO_3$ (BSPT) with grain size ranging from 26 nm to 1.6 μm were investigated in 20 Hz – 55 GHz frequency and 100 K – 500 K temperature ranges. It was found that low-frequency contribution to dielectric permittivity is originating from polar nanoregion-like entities, which are different from conventional ferroelectric domains.
4. For the first time size effect was modelled by means of Effective Medium Approximation (EMA) in case of ferroelectric ceramics without making any assumptions regarding intrinsic properties of the material. In this case BSPT ceramics were studied. It was found that generalised core-shell structure is sufficient to describe properties of the ceramics.
5. For the first time investigation of electrical properties of Ba_2SnO_4 ceramics were performed. No dielectric anomalies in 300 K – 1000 K temperature range were found.

1.3. Statements presented for defence

1. Bulk properties of relaxor materials are heavily influenced by polar nanoregions, but they do not fully determine ground state of the material. Morphology of the material (i.e. grain size of ceramics, thickness of a film) determines growth and interactions of the nanoregions, thus influencing bulk properties.
2. Effective medium approximation can explain evolution of dielectric properties of ferroelectrics and relaxors only if dependence of dielectric properties of inter-grain material on grain size is known.
3. There exist polar entities in ferroelectrics, which are different from ferroelectric domains and are similar to polar nanoregions in relaxors. Their contribution to dielectric permittivity is comparable to all other

contributions, i.e. ferroelctric domains and polar modes. Dimensions of these entities depend on grain size in accordance with Kittel's law.

1.4. List of publications included into the thesis

1. Maksim Ivanov, Juras Banys, C. Bogicevic, Jean-Michel Kiat. Size Effects on Dielectric Properties of Nanograin PSN Ceramics // Ferroelectrics. ISSN 0015-0193 print / 1563-5112 online. 2012, vol. 429, p. 43-47.
2. R. Grigalaitis, M. Ivanov, J. Macutkevic, J. Banys, J. Carreaud, J. M. Kiat, V. V. Laguta, and B. Zalar, Size effects in a relaxor: further insights into PMN // J. Phys.: Condens. Matter. DOI: 10.1088/0953-8984/26/27/272201. 2014, vol. 26, p. 272201.
3. R. M. Katiliute, P. Seibutas, M. Ivanov, R. Grigalaitis, A. Stanulis, J. Banys, and A. Kareiva. Dielectric and Impedance Spectroscopy of $BaSnO_3$ and $Ba2SnO_4$ *// Ferroelectrics. DOI: 10.1080/00150193.2014.892812. 2014, vol. 464, p. 49–58.*
4. J. Scott, H.J. Fan, S. Kawasaki, J. Banys, M. Ivanov, A. Krotkus, J. Macutkevič, R. Blinc, V.V. Laguta, P. Cevec, J.S. Liu, A. Kholkin. Terahertz emission from tubular $Pb(Zr,Ti)O_3$ nanostructures // Nano letters. ISSN: 1530-6984. 2008, vol. 8 (12), p. 4404 — 4409.
5. S Balčiūnas, M Ivanov , R Grigalaitis, J Banys, H Amorín, A Castro and M Algueró, Revisiting the broadband dielectric properties of high sensitivity piezoelectric $BiScO_3$-$PbTiO_3$: size effects // SUBMITTED.

1.5. Other papers

1. J. Banys, M. Ivanov, R. Adomavicius, A. Krotkus, J. Macutkevic, J. Scott, H.J. Fan. THz reflectivity spectroscopy of tubular PZT nanostructures // Integrated Ferroelectrics. ISSN: 1058-4587. 2009, vol.

106 (1), p. 17 — 22.

2. J. Banys, R. Grigalaitis, M. Ivanov, J. Carreaud, J. Kiat. Dielectric behaviour of a nanograin PMN powders // Integrated ferroelectrics. ISSN: 1058-4587. 2008, vol. 99 (1), p. 132 — 139.
3. M. Ivanov, J. Banys, S. Rudys, R. Grigalaitis. Measurements of complex dielectric constant of ferroelectrics with six-port reflectometer in 80-120 GHz frequency range // Ferroelectrics. ISSN: 0015-0193. 2008, vol. 367, p. 229 — 233.
4. J. Banys, S. Rudys, M. Ivanov, J. Li, H. Wang. Dielectric properties of cubic bismuth based pyrochlores containing lithium and fluorine // Journal of the European Ceramic Society. ISSN: 0955-2219. 2010, vol. 30 (2), p. 385 — 388.
5. J. Banys, M. Ivanov, J. Macutkevic, A. Krotkus, H.J. Fan, S. Kawasaki, J.F. Scott. THz Emission from PZT Nanotubes // Ferroelectrics. ISSN: 0015-0193. 2009, vol. 378 (1), p. 79 — 83.
6. M. Ivanov, S. Rudys, S. Lapinskas, J. Banys, J. Macutkevic, A.Y. Yermakov, M.A. Uimin, A.A. Mysik, O. Shenderova. Measurements of complex dielectric permittivity and magnetic permeability of carbon-coated Ni capsules // Microwave Radar and Wireless Communications (MIKON), 2010 18th International Conference on. ISBN: 978-1-4244-5288-0.
7. M. Ivanov , K. Klemkaite, A. Khinsky , A. Kareiva, J. Banys. Dielectric and Conductive Properties of Hydrotalcite // Ferroelectrics. ISSN: 0015-0193 print / 1563-5112 online. 2011, vol. 417 (1), p. 136 – 142.
8. Saulius Rudys , Maksim Ivanov , Juras Banys , Nikolai P. Vyshatko, Aleksandr D. Shilin, Andrei N. Salak. Dielectric and Impedance Spectroscopy of xNBT–(1-x)LMT Ceramics // Ferroelectrics. ISSN: 0015-0193 print / 1563-5112 online. 2011, vol. 417 (1), p. 143 – 150.
9. Š. Svirskas, M. Ivanov, Š. Bagdzevičius, M. Dunce, M. Antonova, E. Birks, A. Sternberg, A. Brilingas J. Banys. Dynamics of Phase

Transition in 0.4NBT-0.4ST-0.2PT Solid Solution // Integrated Ferroelectrics. ISSN 1058-4587 print / 1607-8489 online. 2012, vol. 134, p. 81 – 87.

10. S. Rudys , M. Ivanov, J. Banys. Ansoft HFSS Software Application for the Dielectric and Magnetic Measurements of Ferroelectrics and Related Materials in Microwaves // Ferroelectrics. ISSN: 0015-0193 print / 1563-5112 online. 2012, vol. 430, 115–122
11. Polina P. Kuzhir, Alesia G. Paddubskaya, Mikhail V. Shuba, Sergey A. Maksimenko, Alain Celzard, Vanessa Fierro, Gisele Amaral-Labat, Antonio Pizzi, Gintaras Valušis, Jan Macutkevic, Maksim Ivanov, Juras Banys, Silvia Bistarelli, Antonino Cataldo, Matteo Mastrucci, Federico Micciulla, Immacolata Sacco, Eleonora Stefanutti, Stefano Bellucci. Electromagnetic shielding efficiency in Ka-band: carbon foam versus epoxy/carbon nanotube composites // Journal of Nanophotonics. 2012, vol. 6 (1), p. 061715-061715.
12. R Mackeviciute, M Ivanov, J Banys, Nikola Novak, Zdravko Kutnjak, Magdalena Wencka and J F Scott. The perfect soft mode: giant phonon instability in a ferroelectric //J. Phys.: Condens. Matter. DOI:10.1088/0953-8984/25/21/212201. 2013, vol. 25, p. 212201.
13. Svirskas S, Ivanov M, Bagdzevicius S, Macutkevic J, Brilingas A, Banys J, Dec J, Miga S, Dunce M, Birks E, Antonova M, Sternberg A. Dielectric properties of $0.4Na_{0.5}Bi_{0.5}TiO_3$–$(0.6\text{-}x)SrTiO_3$–$xPbTiO_3$ solid solutions // Acta Materialia. DOI: 10.1016/j.actamat.2013.11.040. 2014, vol. 64, p. 123.
14. T. Šalkus, A. Kežionis, M. Ivanov, M. I. Kayla, M. Kranjčec, I. P. Studenyak, and J. Banys, Electrical conductivity and dielectric permittivity of Cu6AsS5I superionic crystals // Solid State Ionics. DOI: 10.1016/j.ssi.2013.09.057. 2014, vol. 262, p. 582–584.
15. S. Rudys, M. Ivanov, J.Banys. EM simulation for the material electrical properties measurement in microwave range // Acta Universitatis

Ouluensis. ISSN 1796-2226. 2009, vol. 323, p. 73-82.

1.6. Presentations at conferences

2010 - 11 - 26..28 3rd SEMINAR Properies of ferroelectric and superionic systems. Uzhgorod, Ukraine.

1. Maksim Ivanov, Saulius Rudys, Saulius Lapinskas, Juras Banys, Jan Macutkevic, A. Ye. Yermakov, M. A. Uimin, A. A. Mysik, Olga Shenderova: Measurements of complex dielectric permittivity and magnetic permeability of carbon-coated Ni capsules, p. 11.

2011 - 04 - 5...8 Functional materials and nanotechnologies. Riga, Latvia

1. M. Ivanov, M. Kinka, S. Rudys, J. Banys, C. Bogicevic, J.-M. Kiat: Dielectric Properties of Nanograin PSN Ceramics, p. 208.

2. Š. Svirskas, M. Ivanov, Š. Bagdzevičius, J. Banys, M. Dunce, M. Antonova, E. Birks, A. Sternberg, V. Zauls: Dielectric Properties Of 0.4Na1/2Bi1/2TiO3 - (0.6 - X)SrTiO3 - XPbTiO3 Solid Solutions, p. 210.

2011 - 06-26 - 07-01 European Meeting on Ferroelectricity, Bordeaux, France

1. Maksim Ivanov, Martynas Kinka, Saulius Rudys, Juras Banys, C. Bogicevic, Jean-Michel Kiat: Size Effects on Dielectric Properties of Nanograin PSN Ceramics (P5-15)

2. Š. Svirskas, M. Ivanov, Š. Bagdzevičius, J. Banys, M. Dunce, M. Antonova, E. Birks, A. Sternberg: Broadband Dielectric Spectroscopy of 0.4Na1/2Bi1/2TiO3 – (0.6-x)SrTiO3 – xPbTiO3 Solid Solutions (P3-12)

2011 - 07-31 - 08-4 ISIF 2011 (International Symposium on Integrated Functionalities), Cambridge, United Kingdom

1. Maksim Ivanov, Juras Banys, C. Bogicevic, Jean-Michel Kiat:

Dielectric Spectroscopy of Nanograin PSN Ceramics, p. 125.

2. Š. Svirskas, M. Ivanov, Š. Bagdzevičius, J. Banys, M. Dunce, M. Antonova, E. Birks, A. Sternberg: Investigation of 0.4Na1/2Bi1/2TiO3-(0.6-x)SrTiO3-xPbTiO3 Solid Solutions, p. 109.

2011 - 10 - 6..8 39-oji Nacionalinė Fizikos Konferencija, Vilnius, Lithuania

1. Maksim Ivanov, Saulius Rudys, Saulius Lapinskas, Juras Banys, Jan Macutkevic, A. Ye. Yermakov, M. A. Uimin, A. A. Mysik, Olga Shenderova: Dielectric and magnetic properties of carbon-coated nickel capsules in wide microwave frequency range, p. 51.

2. Maksim Ivanov, Martynas Kinka, Saulius Rudys, Juras Banys, C. Bogicevic, Jean-Michel Kiat: Dielectric Properties of Nanograin PSN Ceramics, p. 52.

3. Š. Svirskas, M. Ivanov, Š. Bagdzevičius, J. Banys, M. Dunce, M. Antonova, E. Birks, A. Sternberg: Broadband Dielectric Spectroscopy of 0.4Na1/2Bi1/2TiO3 – (0.6-x)SrTiO3 – xPbTiO3 Solid Solutions, p. 98.

4. Saulius Rudys, Maksim Ivanov, Juras Banys, Nikolai P. Vyshatko, Andrei N. Salak: Dielectric and Impedance spectroscopy of xNBT-(1-x)LMT Ceramics, p. 178.

5. Maksim Ivanov, Juras Banys, Saulius Rudys, Jing Li, Hong Wang: Dielectric spectroscopy of Bi1.5ZnNb1.5O7-xF2x (x=0.1, 0.2 and 0.4) ceramics, p. 179.

2011 - 10 - 14 10th International Conference of Lithuanian Chemists "CHEMISTRY 2011", Vilnius, Lietuva

1. Maksim Ivanov, Kristina Klemkaite, Alexander Khinsky, Aivaras Kareiva, Juras Banys: Dielectric and Conductive Properties Of Hydrotalcite

2. Š. Svirskas, M. Ivanov, Š. Bagdzevičius, J. Banys, M. Dunce, M. Antonova, E. Birks, A. Sternberg, V.Zauls: Dielectric Properties Of

0.4Na1/2Bi1/2TiO3 – (0.6 – X)SrTiO3 - XPbTiO3 Solid Solutions

2011 - 11 - 16..18 9th Students' Meeting and 2nd ESR COST MP0904 Workshop, Novi Sad, Serbia

1. M. Ivanov, S. Rudys, J. Banys, C. Bogicevic, J.-M. Kiat: Dielectric Spectroscopy of Nanograin PSN Ceramics, p. 115.

2012 - 03 - 12..13 COST MP0904 Training School "Nanostructured oxides: from laboratory research to industrial applications", Genoa, Italy

1. M. Ivanov, S. Rudys, J. Banys, C. Bogicevic, J.-M. Kiat: Dielectric Spectroscopy of Nanograin PSN Ceramics

2012 - 03 - 13..16 ICWNCN-2012 International Conference and Workshop on Nanostructured Ceramics and other Nanomaterials, Delhi, India

1. S. Rudys, M. Ivanov, R. Grigalaitis, S. Svirskas, A. Mikonis, T. Ramoska, J. Banys: Broadband dielectric spectroscopy of ferroelectrics and related materials

2. Juras Banys, Robertas Grigalaitis, Saulius Rudys, Maksim Ivanov, Nikolai P. Vyshatko, Aleksandr D. Shilin, Andrei N. Salak: Meyer-Neldel Rule for Electrical Conductivity in xNBT-(1-x)LMT Ceramics

2012 - 04 - 09..20 Advanced Research Workshop Multiferroic and Multifunctional Materials MMM-2012, Natal - RN - Brazil

1. Ruta Mackeviciute, Maksim Ivanov, Juras Banys, Jose Antonio Eiras: Broadband dielectric spectroscopy of PFW ceramics doped with manganese oxide, p. 82.

2012 - 04 - 17..20 Functional materials and nanotechnologies. Riga, Latvia

1. Š. Svirskas, M. Ivanov, Š. Bagdzevičius, J. Banys, M. Dunce, M.

Antonova, E. Birks, A. Sternberg: Dynamics of Phase Transition in 0.4Na1/2Bi1/2TiO3 – (0.6-x)SrTiO3 – xPbTiO3 Solid Solutions, p. 140

2012 - 04 - 23 The Third COST MP0904 WG Workshop “Advanced characterization and functional properties of ferroelectrics and multiferroics”, Vilnius, Lithuania

1. Šarūnas Svirskas, Maksim Ivanov, Šarūnas Bagdzevičius, Jūras Banys, Marija Dunce, Maija Antonova, Eriks Birks, Andris Sternberg: DYNAMICS OF PHASE TRANSITION IN 0.4Na0.5Bi0.5TiO 3 -(0.6-x)SrTiO3-xPbTiO3.

2012 - 05 - 21..25 XX Polish - Czech seminar "Structural & Ferroelectric Phase Transitions", Ustron, Poland

1. Ruta Mackeviciute, Maksim Ivanov, Juras Banys, Jose Antonio Eiras: Dielectric properties of P(F1/2W1/2)O3+1%Mn)2 ceramics, p. 109.

2. Š. Svirskas, M. Ivanov, Š. Bagdzevičius, J. Banys, M. Dunce, M. Antonova, E. Birks, A. Sternberg: Dynamics of Phase Transition in 0.4Na1/2Bi1/2TiO3 – (0.6-x)SrTiO3 – xPbTiO3, p. 23.

2012 - 07 - 9..13 ISAF ECAPD PFM 2012, Aveiro, Portugal

1. Maksim Ivanov, Juras Banys, Satoshi Wada: BROADBAND DIELECTRIC PROPERTIES OF 0.5BaTiO3–0.5KNbO3 COMPOSITE

2. Saulius Rudys, Maksim Ivanov, Juras Banys, Robertas Grigalaitis, Nikolai P. Vyshatko, Aleksandr D. Shilin, Andrei N. Salak: MEYER-NELDEL RULE FOR ELECTRICAL CONDUCTIVITY OBSERVATION IN xNBT–(1-x)LMT CERAMICS

2012 - 08 - 20..24 ISFD-11-RCBJSF, Ekaterinburg, Russia

1. Š. Svirskas, M. Ivanov, Š. Bagdzevičius, J. Banys, M. Dunce, M. Antonova, E. Birks, A. Sternberg: Dielectric Dispersion and Phase Diagram of 0.4NBT-(0.6-x)ST-xPT Ceramics, p. 47.

2. M. Ivanov, S. Wada, J. Banys: Broadband dielectric properties of 0.5BaTiO3–0.5KNbO3 composite, p. 150.

2012 - 09 - 09..13 II Ukrainian-Polish-Lithuanian Meeting on Ferroelectrics Physics, Lviv, Ukraine

1. Šarūnas Svirskas, Maksim Ivanov, Šarūnas Bagdzevičius, Jūras Banys, Marija Dunce, Maija Antonova, Eriks Birks, Andris Sternbergs: Distribution of relaxation times in 0.4Na0.5Bi0.5TiO3-(0.6-x)SrTiO3-xPbTiO3 solid solutions, p. 2.

2. M. Ivanov, S. Wada, J. Banys: Broadband dielectric properties of 0.5BaTiO3–0.5KNbO3 composite, p. 63.

2012 - 09 - 24..26 Conference COST MPO904 Action „Single & and multiphase ferroics and multiferroics with restricted geometries” & IEEE ROMSC 2012, Iasi, Romania

1. M. Ivanov, S. Balčiūnas, R. Grigalaitis, H.Amorín, A. Castro, M. Algueró, J. Banys: Dielectric permittivity of nanostructured BSPT ceramics, p. 63.

2012 - 11 - 19..21 COINAPO 2012 Meeting "Nanocomposites of inorganic fullerenes/nanotubes, their characterization, properties & testing", Rehovot, Israel

1. M. Ivanov, J. Macutkevic, J. Banys, P. Kuzhir, A. Paddubskaya, S. Maksimenko, L. Coderoni, F. Micciulla, I. Sacco, S. Bellucci: Dielectric spectroscopy of epoxy resin composite with carbon nanotubes inclusions, p. 102.

2013 - 03 - 21 ..22 MP0904 WG1 Meeting, Belfast, United Kingdom

1. M. Ivanov, S. Balčiūnas, R. Grigalaitis, H.Amorín, A. Castro, M. Algueró, J. Banys: Dielectric permittivity of nanostructured BSPT ceramics

2013 - 03 - 21..24 Functional materials and nanotechnologies. Tartu, Estonia

1. S. Balčiūnas, R. Mackevičiūtė, M. Ivanov, H.Amorín, A. Castro, M. Algueró, J. Banys: DIELECTRIC PROPERTIES OF NANOGRAIN BSPT CARAMICS, p. 134.

2. Kęstutis Bučinskas, Rūta Mackevičiūtė, Maksim Ivanov, Robertas Grigalaitis, Jūras Banys, Eva Sapper, Jürgen Rödel: DIELECTRIC AND IMPEDANCE SPECTROSCOPY OF Fe DOPED 0.94(Na0.5Bi0.5TiO3)-0.06BaTiO3 CERAMICS, p. 203.

2013 - 05 - 27..31 E-MRS 2013 Spring Meeting, Strasbourg, France

1. M. Ivanov, S. Balčiūnas, J. Banys; H.Amorín, A. Castro, M. Algueró: Dielectric permittivity of nanostructured BSPT ceramics

2013 - 06 - 10..12 40-oji Lietuvos Nacionalinė Fizikos Konferencija, Vilnius, Lithuania.

1. T. Šalkus, A. Kežionis, M. Ivanov, A. F. Orliukas, M. Kranjčec, M. Kayla, I. Studenyak: Electrical conductivity and dielectric permittivity of Cu6PAsS5I superionic crystals, p. 42.

2. M. Ivanov, S. Wada, J. Banys: Broadband dielectric properties of 0.5BaTiO3–0.5KNbO3 composite, p. 55.

3. S. Balčiūnas, M. Ivanov, H. Amorín, A. Castro, M. Algueró, J. Banys: Dielectric properties of nanostructured BSPT ceramics, p. 56.

4. M. Ivanov, K. Bučinskas, J. Banys, E. Sapper, J. Rödel: DIELECTRIC AND IMPEDANCE SPECTROSCOPY OF Fe DOPED 0.94(Na0.5Bi0.5TiO3)-0.06BaTiO3 CERAMICS, p. 57.

5. I. Kranauskaitė, M. Ivanov, Š. Bagdzevičius, K. Bormanis, J. Banys: Broadband dielectric investigation of (Sr1-1.5xBix)TiO3 (x=0.15, 0.1, 0.05), p. 87.

2013 - 07 - 21..25 Joint UFFC, EFTF and PFM Symposium, Prague, Czech Republic

1. Kęstutis Bučinskas, Maksim Ivanov, Robertas Grigalaitis, Jūras Banys, Eva Sapper, Jürgen Rödel: DIELECTRIC AND IMPEDANCE SPECTROSCOPY OF Fe DOPED 0.94(Na0.5Bi0.5TiO3)-0.06BaTiO3 CERAMICS (ISAF-P1A-40).

2. Šarūnas Svirskas, Maksim Ivanov, Šarūnas Bagdzevičius, Jūras Banys, Jan Dec, Seweryn Miga, Marija Dunce, Eriks Birks, Maija Antonova, Andris Sternbergs: Linear and Nonlinear Dielectric Properties of Ternary Solid Solutions 0.4Na0.5Bi0.5TiO3-(0.6-x)SrTiO3-xPbTiO3 (ISAF-P3C-38).

2013 - 09 - 01..06 International Meeting of Ferroelectricity, Krakow, Poland

1. R. Mackeviciute, M. Ivanov, J. Banys, J. F. Scott: BROAD BAND DIELECTRIC INVESTIGATION OF TSCC SINGLE CRYSTAL, p. 359.

2. Šarūnas Svirskas, Maksim Ivanov, Jūras Banys, Marija Dunce, Maija Antonova, Eriks Birks, Andris Sternbergs: DIELECTRIC SPECTROSCOPY OF TERNARY SOLID SOLUTION (0.4-y)NBT-0.6ST-yPT, p. 414.

3. M. R. Katiliute, P. Seibutas, M. Ivanov, R. Grigalaitis, A. Stanulis, J. Banys, A. Kareiva: DIELECTRIC AND IMPEDANCE SPECTROSCOPY OF BaSnO3 AND BaSn2O4, p. 504.

4. S. Balčiūnas, M. Ivanov, H.Amorín, A. Castro, M. Algueró,J. Banys: DIELECTRIC PROPERTIES OF NANOGRAIN BSPT CERAMICS, p. 573.

2013 - 09 - 15..19 dyProSo XXXIV (Dynamical Properties of Solids), Vienna, Austria

1. Mackeviciute, Ruta; Ivanov, Maksim; Banys, Juras; Scott, James: Broad band dielectric investigation of TSCC single crystals, p. 111.

2. Ivanov, Maksim; Bucinskas, Kestutis; Banys, Juras; Kazakevicius,

Edvardas; Sapper, Eva; Rödel, Jürgen: Dielectric and impedance spectroscopy of relaxor 0.94(Na0.5Bi0.5TiO3)-0.06BaTiO3 ceramics, p. 133.

3. Jablonskas, Dziugas; Lapinskas, Saulius; Rudys, Saulius; Ivanov, Maksim; Banys, Juras: Multimode finite space model for open-ended coaxial line dielectric spectroscopy, p. 146.

2013 - 11 - 06..09 The Tenth Students Meeting and The Third Workshop for Early Stage Researchers – COST MP0904

1. S. Balčiūnas,M. Ivanov,H. Amorín, A. Castro, M. Algueró, J. Banys: DIELECTRIC PROPERTIES OF NANOGRAIN BSPT CERAMICS, p. 126.

2. Š. Svirskas, A. Olšauskaitė,M. Ivanov, J. Banys, J. Dec, S. Miga,M. Dunce, E. Birks, M. Antonova, A. Sternberg: BROADBAND DIELECTRIC SPECTROSCOPY OF A-SITE SUBSTITUTED PEROVSKITE CERAMICS, p. 129.

2014 - 01 - 26..29 2014 Workshop on the Fundamental Physics of Ferroelectrics and Related Materials

1. S. Balčiūnas,M. Ivanov,H. Amorín, A. Castro, M. Algueró, J. Banys: Size effect and contribution of domain walls to dielectric properties of BSPT ceramics, p. 118.

2014 - 06 - 16..19 14th edition of ELECTROCERAMICS Conference (Bucharest, Romania)

1. Kęstutis Bučinskas, Maksim Ivanov, Edvardas Kazakevičius, Jūras Banys, Eva Sapper, Jürgen Rödel: Dielectric and Impedance Spectroscopy of NBT-xBT Ceramics, p. 98.

2. S. Balčiūnas, M. Ivanov, R. Grigalaitis, H.Amorín, A. Castro, M. Algueró, J. Banys: Size effects and contribution of domain walls to dielectric properties of BSPT ceramics, p. 434.

2014-07 - 07..11 European Conference on Application of Polar Dielectrics 2014 (Vilnius, Lithuania)

1. M. Ivanov, S. Balčiūnas, H.Amorín, A. Castro, M. Algueró, J. Banys: Grain Size Effect on Dielectric Permittivity of 0.36BiScO3 – 0.64PbTiO3 Perovskite Ceramics, p. 81.

2. A.Olšauskaitė, Š. Svirskas, M. Ivanov, T. Šalkus, A. Kežionis, J. Banys, M. Dunce, E. Birks, M. Antonova, A. Sternberg: Broadband dielectric spectroscopy of xNa0.5Bi0.5TiO3-(1-x)Sr0.7Bi0.2TiO3 solid solutions, p. 126.

3. R. Mackeviciute, R. Grigalaitis, M. Ivanov, R. Sliteris, J. Banys: Dielectric and pyroelectric properties of PMN-29PT single crystal near MPB, p. 131.

2014 - 08 - 31 .. 09 - 04 III Polish-Lithuanian-Ukrainian Meeting on Ferroelectrics Physics (Wroclaw, Poland)

1. M. Ivanov, R. Grigalaitis, J. Macutkevič, J. Banys: DIELECTRIC PROPERTIES OF FERROELECTRIC RELAXORS: SIZE EFFECTS (O-INV-17).

2. Overview

2.1. Dynamics of dielectric permittivity of uniform media

Dielectric permittivity can be understood in several ways. Firstly, it shows how much the external field is diminished inside dielectric. However, this reduction of field is related to orientation of dipoles, which compensate the field. Thus, dielectric permittivity is also a measure of polarisability of the material.

All is easy when field is static, but things get complicated when external electric field becomes alternating. It will force the dipoles move accordingly, but charged particles have mass, so they bound to have inertia and might not always be able to respond to the external stimulus with the required speed.

The most important charged particles inside the material are electrons and ions. At least some electrons are bound to their atom or ion, and if external field is small their bond might be considered as a spring. With the mass of the electron this system forms a resonant mechanical system. Movement of the system in response to external field is the limiting factor for dielectric permittivity. The same situation is in case of movement of ions in a local potential. Frequency dependence of dielectric constant in such systems is described by the following equation:

$$\varepsilon(\omega) = \varepsilon' - \mathrm{i}\,\varepsilon'' = \varepsilon_\infty + \frac{\Delta\varepsilon \cdot \omega_0^2}{\omega_0^2 - \omega^2 + \mathrm{i}\,\gamma\omega} \qquad (1)$$

Here, ε_∞ is contribution of all higher frequency processes and is equal to 1 in case of the fastest process, $\Delta\varepsilon$ is dielectric strength of the process, ω_0 is angular resonance frequency (usually is observed at frequencies higher than 1 THz), γ is damping, ω is angular frequency of the external field.

As we can see, the permittivity has both real and imaginary values. The latter are a mathematical simplification and are associated with losses in the

system or might be interpreted as (optical) conductivity. Both are valid.

In case of high damping or when the local potential of charged particle allows hopping of the ion, then formula (1) can be transformed to Debye formula:

$$\varepsilon(\omega)=\varepsilon_{\infty}+\frac{\Delta\varepsilon}{1+\mathrm{i}\omega\tau} \tag{2}$$

Here, τ is the relaxation time of the system. The relaxation time usually corresponds to frequencies lower than 1 THz. Relaxational type of dispersion will be the most relevant to the current work.

The two previous types of dispersions are the limiting (idealised) forms. Very often distributions of characteristic times are important to be taken into account. The origin of the distribution can be some type of disorder in the system, e.g. compositional in case of solid solutions.

In many cases relaxational process with a distribution of relaxation times can be modelled by either Cole-Cole (eq. (3), [1]) or Havriliak-Negami (eq. (4), [2]) equations.

$$\varepsilon(\omega)=\varepsilon_{\infty}+\frac{\Delta\varepsilon}{1+(\mathrm{i}\omega\tau)^{1-\alpha}} \tag{3}$$

$$\varepsilon(\omega)=\varepsilon_{\infty}+\frac{\Delta\varepsilon}{\left(1+(\mathrm{i}\omega\tau)^{1-\alpha}\right)^{\beta}} \tag{4}$$

Here parameter α defines width of the distribution of relaxation times, and β defines asymmetry of the distribution. It is important to note, that the time parameter in (3) is the mean relaxation and the most probable relaxation time, but it is neither in case of Havriliak-Negami formula (4). However, it is possible to calculate both 1st and 2nd order moments [3]. In cases when predefined formulas do not work it is possible to find distribution of relaxation times:

$$\varepsilon(\omega)=\varepsilon_{\infty}+\Delta\varepsilon\int_{-\infty}^{\infty}\frac{f(\ln\tau)\,\mathrm{d}\ln\tau}{1+\mathrm{i}\omega\tau} \tag{5}$$

Here $f(\ln\tau)$ is the distribution of relaxation times. Very often formula (3) is sufficient to describe dielectric spectra of a particular material.

2.2. Effective medium approximation

In inhomogeneous systems the dielectric properties might be very different from properties of constituent parts. It is analytically easy to analyse systems in the limit of small inhomogeneities, where the probing electric field can be assumed constant in individual homogeneous parts or components of the system. This is so-called quasistatic or effective-medium approximation (EMA) in which the magnetic field effects (e.g. eddy currents) can be neglected. The EMA is justified as long as the wavelength of the probing wave is much larger than the individual homogeneous parts and in the case of absorbing parts also the local penetration lengths should be much larger than the sizes of all the parts [4].

In this approximation it has a good meaning to introduce the effective dielectric function of the whole system, which is the quantity usually measured in a macroscopic experiment.

2.2.1 General case

It is not easy to calculate effective dielectric permittivity in the most general case, as the value depends not only on dielectric permittivity of different parts and their volume fractions, but also on geometry of inclusions. In case of two components with dielectric permittivities ε_1 and ε_2, effective response can be represented by a sum of three parts [5], [6]:

$$\varepsilon = V_1\varepsilon_1 + V_2\varepsilon_2 + \int_0^1 v_{12}(n')\frac{\varepsilon_1\varepsilon_2}{(1-n')\varepsilon_2 + n'\varepsilon_1}\,\mathrm{d}n'$$

$$V_1 + V_2 + \int_0^1 v_{12}(n')\,\mathrm{d}n' = 1 \qquad (6)$$

$$V_1 + \int_0^1 (1-n')\cdot v_{12}(n')\,\mathrm{d}n' = x_1 \qquad V_2 + \int_0^1 n'\cdot v_{12}(n')\,\mathrm{d}n' = x_2$$

Here, x_1 and x_2 are volume fractions of the components, V_1 and V_2 are volumes of macroscopically percolating clusters and $v_{12}(n')$ is proportional to density of second component clusters inside the first component which are

characterised by a depolarisation factor *n*'. The depolarisation factor shows how many times the internal field in the inclusion is smaller than in the surrounding composite due to charges bound to the surface of the inclusion.

This approach, first proposed by Bergman [6], assumes that boundaries between the components do not move and this is valid for composites, powders and polycrystalline ceramics. It is interesting to note, that permittivity can be substituted by conductivity or even magnetic permeability without loss of generality.

There are quite a few models which work in different situations – at low concentrations, near percolation threshold, special geometries, etc. However, only models suitable for ceramics are of interest in this work.

2.2.2 Brick-layer and core-shell models

There are two major models employed to model dielectric response of ceramics: brick-layer (brick wall) and core-shell (coated spheres) models.

The brick-layer model (BLM) assumes that grains of ceramics are cubes which are separated by a thin layer of a material (inter-grain medium, or grain boundary) with different dielectric properties (figure 2.2.1).

The impedance of composite medium is given by:

$$Z_m = \frac{1}{\frac{1}{Z_i^{\parallel}} + \frac{1}{Z_i^{\perp} + Z_c}} \tag{7}$$

Here, Z_m is the effective complex impedance, $Z_i^{\parallel}$ is the complex impedance of the square pipe, Z_c of the cubic brick, $Z_i^{\perp}$ of the end caps.

It can be shown by mathematical transformation of equation (7), that dielectric permittivity can be expressed as:

$$\varepsilon_m = \varepsilon_i \left[1 + \frac{(\varepsilon_c - \varepsilon_i) x_c}{\varepsilon_c - (\varepsilon_c - \varepsilon_i) x_c^{1/3}} \right] \tag{8}$$

Here, x_c is volume fraction of the cube material (grain material).

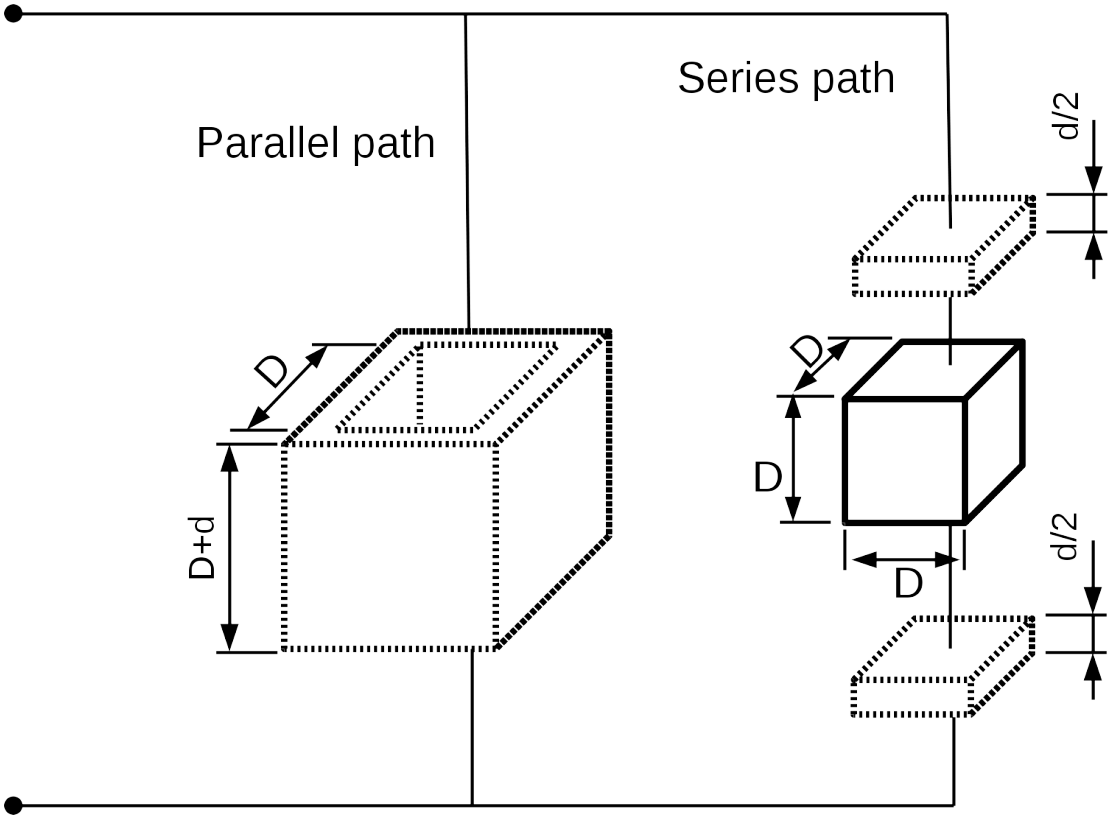

Figure 2.2.1. The microstructure for the Brick Layer Model.

One of the biggest problems of this brick layer model is that it assumes 2D connectivity of the constituents, but in reality the grains are 3D objects. As a result, this model works well only for relatively big grains, which are much bigger than thickness of the inter-grain medium. This can be taken into account, though, through finite element method or making a few more assumptions which are relevant for nanograined ceramics [7].

Another model, core-shell model, was first suggested by Maxwell and Wagner and later confirmed by Hashin and Strikman [8]. The model is sometimes known as Maxwell-Wagner/Hashin-Strikman model (MW-HS). They calculated effective permittivity for the system with macroscopic structure depicted in figure 2.2.2 as:

$$\varepsilon = \varepsilon_s + \frac{x_c}{\frac{1}{\varepsilon_c - \varepsilon_s} + \frac{1 - x_c}{3\varepsilon_s}} \tag{9}$$

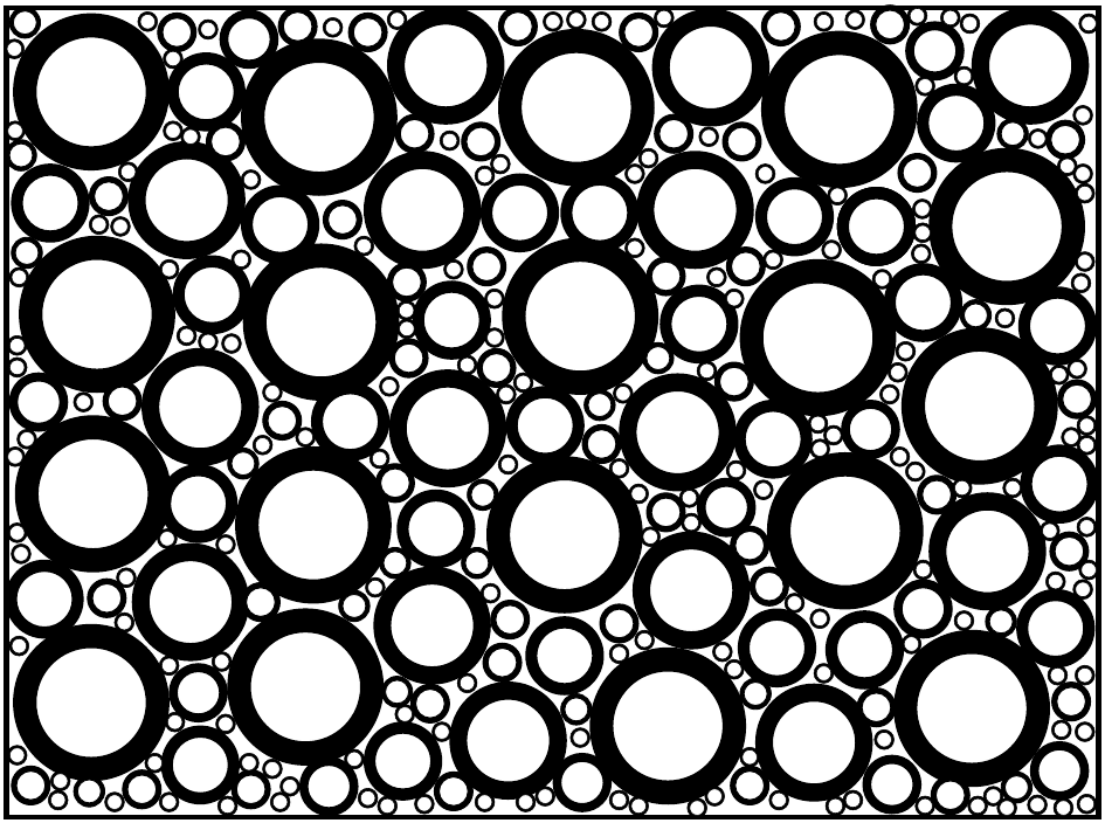

Figure 2.2.2. Core-shell (coated spheres) microstructure. Black denotes coating material, white – core material.

Here, x_c is volume fraction of the core material, ε_c is dielectric permittivity of the core material, ε_s is dielectric permittivity of the shell.

The biggest problem of this composite structure is that it assumes an infinite number of spheres, some being infinitesimally small, occupying all volume, and thickness of the shell is always the same fraction of the diameter of the particle.

It is interesting, that both of the presented models can be unified into a single one, which is known as a generalised core-shell model (also known as a generalised brick-wall model) [9], which is valid for densely packed cores of any shape separated by thin shells. The relation between intrinsic properties and effective (experimentally determined) dielectric permittivity is as follows:

$$\varepsilon = \varepsilon_s \frac{x-n}{1-n} + \frac{1-x}{1-n} \cdot \frac{\varepsilon_c \varepsilon_s}{(1-n)\varepsilon_s + n\varepsilon_c} \tag{10}$$

Here, ε_s is dielectric permittivity of the shell material, ε_c is dielectric permittivity of the bulk (core) material, x is volume fraction of the shell, parameter $n = x/3$ takes into account geometry of the composite (0-3 connectivity).

2.3. Ferroelectricity

Ferroelectric materials are the ones exhibiting spontaneous polarization (alignment of electric dipoles), which is switchable by external electric field. It is important to understand that "spontaneous" means "in the absence of external electric field", and "switchable" means that there are at least 2 different allowed directions (e.g. "up" and "down") in the absence of the field, and the direction can be changed by external field. This nonlinear behaviour was first observed in rochelle salt in 1921 by Valasek [10], and is the first ferroelectric material ever investigated.

2.3.1 Properties of ferroelectric materials

Importance of ferroelectricity lies not only in the switchable polarization, but also in other, related functionalities. For example, all ferroelectrics are pyroelectrics, and all pyroelectrics are piezoelectrics. This allows to use the same material as temperature or mechanical sensor or as an actuator or transducer.

Another important factor is dielectric permittivity of ferroelectric materials. Usually this family of materials exhibits high values of relative dielectric permittivity, which can reach up to 10^5 near ferroelectric to paraelectric phase transition. Temperature dependence of dielectric permittivity is described by Curie-Weiss law in paraelectric state [11]:

$$\varepsilon = \frac{C}{T - T_C} \tag{11}$$

Here, C is Curie-Weiss constant, T_C is the ferroelectric to paraelectric

phase transition temperature. As we can see, permittivity should diverge in the point of phase transition, but this phenomenon is never observed. The reason lies in many assumptions needed to derive formula (11). Firstly, there are no ideal crystals in reality, as ideal crystal needs to be infinite in all dimensions. Secondly, it is nearly impossible to make a real sample without any defects inside it. Thus the permittivity has a peak, but it is finite.

Situation is a little more complicated in the ferroelectric phase. The contribution of ionic vibrations should again follow Curie-Weiss law, albeit with a different Curie-Weiss constant. The new constant would be of different sign and its magnitude would normally be at least twice smaller. However, a different contribution to dielectric permittivity might become relevant.

2.3.2 Domains and domain walls

Ferroelectrics, similarly to ferromagnetic materials, are expected to be polarised in the same direction throughout whole volume. However, these ferroic materials prefer a state with various parts of the crystal having different directions if the crystal is of finite size. This was first described by Kittel [12] and is now known as polydomain state. Domains are continuous areas of the materials which have the same (uniform) polarization. The domains form a particular pattern depending on configuration of the crystal. A few possible domain configurations in a freestanding ferroelectric film or slab are presented in figure 2.3.1.

This periodic structure is there for energetic reasons. The first problem is that ferroelectric materials are insulators. If left alone then charges would gather at places were polarization is not parallel to the surface. This would produce a field, which would be directed to the opposite direction of the polarization. This field is known as a “depolarising” field, as it is acting in the opposite direction. In many ferroelectrics this field is higher than coercive field, making ferroelectric state energetically unfavourable. However, breaking

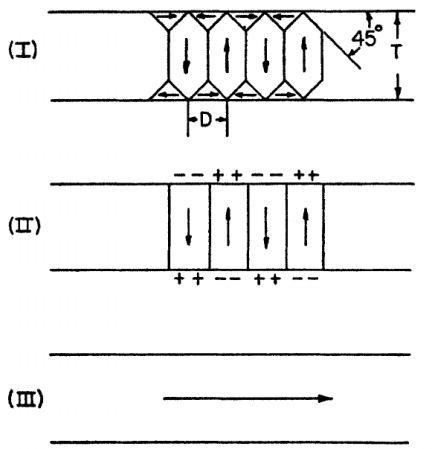

Figure 2.3.1. Domain configurations in freestanding films and slabs.

of the crystal into domains makes the net depolarising field equal to zero. The problem is the area separating the domains, known as “domain wall”.

The spontaneous polarization arises due to spontaneous shift of one or several ions in the crystal structure (see structures S_A and S_B in figure 2.3.2). The actual shift may be very small relative to the lattice size, but it results in absence of a center of symmetry. The domain wall (dashed line in figure 2.3.2, left) might be very narrow, in reality comparable to the lattice size. The domain wall thickness cannot be infinitesimal, though, as nearest neighbour dipoles interact with each other, and dipoles close to the domain wall centre would have smaller shifts. This means that the domain wall contains strained unit cells, which are not at their lowest energy, thus each domain wall costs energy.

Kittel considered both energy of depolarising field and of domain walls in a ferromagnetic film or slab (which is the same for ferroelectric case) and found that there is a certain configuration which is energetically most favourable. He found that stripe domains are the most favourable (infinite in one direction), and their size should be periodic with width of domains equal to

$$D=\sqrt{\frac{\sigma}{U}T} \tag{12}$$

Here, D is domain width, σ is domain wall energy density (per unit area), U is domain energy density (per unit volume), T is thickness of the film or slab.

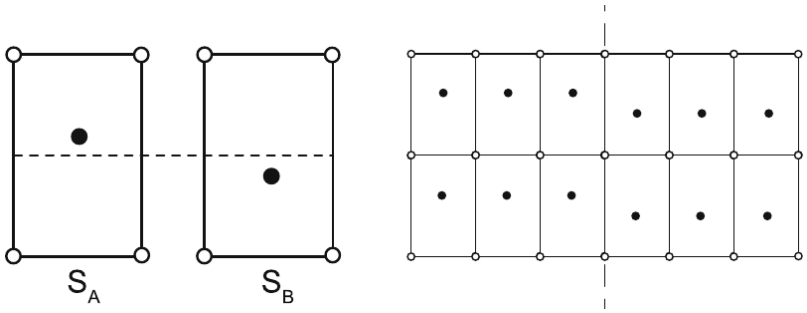

Figure 2.3.2. Simple case of two ferroelectric domain states formed in a crystal lattice.

Size of the domains can be ranging from hundreds of nanometers to hundreds of microns depending on boundary conditions, size of the crystal, etc. However, the possible polarization directions inside domains is limited by crystal symmetry. For example there are only 2 possible directions in situation depicted in figure 2.3.2. More information regarding relation between crystal symmetry and polarization directions can be found in [13], [14].

However, domain patterns are highly periodic only in the static limit. In case of alternating small electric field the domains would respond to it by changing size. The more energy favourable domains would grow at the expense of less favourable ones. This is very often considered as movement of domain walls, as it is the same from mathematical point of view. This movement of domain walls would change net polarization of the crystal in response to external field in a quasi-linear fashion if the field is small. This change in polarization can be associated with dielectric permittivity. It means that domain walls may give additional contribution to the total dielectric permittivity of the material. The contribution might be quite big (i.e. [15], [16]), sometimes exceeding other contributions by orders of magnitude [17], [18]. However, this contribution is associated with a huge amount of atoms, and it is relatively slow. Contributions of ions usually have their characteristic frequencies in THz or far infrared range. However, it lies in radio- and microwave range in case of domains.

2.4. Ferroelectric relaxors

Ferroelectric relaxors (also known as “relaxor ferroelectrics” or simply “relaxors” for short) are a class of disordered crystals possessing peculiar structure and properties. Relaxor ferroelectrics found many applications in electronics such as multilayer ceramic capacitors, electro-optical devices, and medical imaging devices [19]. At high temperature they exist in a non-polar paraelectric phase, which is similar in many respects to the paraelectric phase of normal ferroelectrics. Upon cooling they transform into the ergodic relaxor state in which polar regions of nanometer scale (polar nano regions, or PNRs for short) with randomly distributed directions of dipole moments appear. This transformation which occurs at the so-called Burns temperature (T_B) [20] cannot be considered a structural phase transition because it is not accompanied by any change of crystal structure on the macroscopic or mesoscopic scale. Nevertheless, the polar nanoregions affect the behaviour of the crystal dramatically, giving rise to unique physical properties. For this reason the state of materials at $T < T_B$ is often considered as the new phase different from the paraelectric one. At temperatures close to T_B the polar nanoregions are mobile and their behaviour is ergodic. On cooling, their dynamics slows down enormously and at a low enough temperature, T_0 (typically hundreds degrees below T_B), the polar nanoregions in the canonical relaxors become frozen into a nonergodic state, while the average symmetry of the crystal still remains cubic.

Similar kind of nonergodicity is characteristic of a dipole glass (or spin glass) phase. The existence in relaxors of an equilibrium phase transition into a low-temperature glassy phase is one of the most interesting hypotheses which has been intensively discussed. Freezing of the dipole dynamics is associated with a large and wide peak in the temperature dependence of the dielectric permittivity with characteristic dispersion observed at all frequencies practically available for dielectric measurements. Usually, the peak value of

dielectric permittivity for relaxors is very high (more than 10000), similarly as in the ferroelectrics, but in contrast to ferroelectrics the dielectric anomaly is highly broadened and its temperature shifts with frequency due to the dielectric dispersion [21]. Similarly, as in typical displacive ferroelectrics, the soft phonon modes also exist in ferroelectric relaxors [22]. The critical temperature of the soft phonon modes is close to T_B and the soft mode is ferroelectric soft mode inside polar nanoregions. Moreover, it was observed that strong electric bias field can induce typical displacive ferroelectric phase transition by means of Raman, polarization hysteresis and calorimetric measurements [23], [24]. Nevertheless, contribution of the soft phonon modes to the static dielectric permittivity of relaxors without bias electric field is quite low and no dielectric anomaly was observed in the temperature dependence of the static dielectric permittivity of ferroelectric relaxors close to T_B [25]. Moreover, the nonergodic relaxor state existing below T_0 can be irreversibly transformed into a ferroelectric state by a sufficiently strong external electric field. This is an important characteristic of relaxors which distinguishes them from typical dipole glasses. Upon heating the ferroelectric phase transforms to the ergodic relaxor one at the temperature T_C which is very close to T_0. In some relaxors the spontaneous (i.e. without the application of an electric field) phase transition from the ergodic relaxor into a low-temperature ferroelectric phase still occurs at T_C and thus the nonergodic relaxor state does not exist.

Compositional disorder, i.e. the disorder in the arrangement of different ions on the crystallographically equivalent sites, is the common feature of relaxors. The relaxor behaviour was first observed in the perovskites with disorder of non-isovalent ions, including the stoichiometric complex perovskite compounds, e.g. $Pb(Mg_{⅓}Nb_{⅔})O_3$ (PMN) [26] or $Pb(Sc_{½}Ta_{½})O_3$ (PST)[27] (in which Mg^{2+}, Sc^{3+}, Ta^{5+} and Nb^{5+} ions are fully or partially disordered in the B-sublattice of the perovskite ABO_3 structure) and nonstoichiometric solid solutions, e.g. $Pb_{1-x}La_x(Zr_{1-y}Ti_y)_{1-x/4}O_3$ (PLZT) [28], [29] where the substitution of La^{3+} for Pb^{2+} ions necessarily leads to vacancies on the A-sites. Recently an

increasing amount of works on lead-free disordered piezoelectrics has shown that many homovalent solid solutions, e.g. $Ba(Ti_{1-x}Zr_x)O_3$ (BTZ) [30], [31], and $Ba(Ti_{1-x}Sn_x)O_3$ [32] can also exhibit relaxor behaviour.

The current research activity in relaxor physics is mostly concentrated on differences and similarities between the relaxors, the ferroelectrics and the dipolar glasses. It was demonstrated for example that the dipolar glasses can be obtained by doping of relaxors [33]. On the other hand the differences between the relaxors and the displacive ferroelectrics recently were explained by a phonon localization idea [34]. Moreover, the formation of polar nanoregions was attributed to intrinsic local modes in terms of discrete breathers [34]–[36]. Thus, the existence of such modes should be the main difference between the relaxors and the displacive ferroelectrics [35]. The differences between various ferroic systems becomes very important in the case of new disordered materials [37].

The Vogel-Fulcher law is a common characteristic of relaxor and dipolar glasses [33]. It can be applied for relaxation time:

$$\tau = \tau_0 \exp\left(\frac{E_A}{k_B\left(T - T_0\right)}\right) \tag{13}$$

where τ_0 is the attempt relaxation time, E_A – activation energy, T_0 - freezing temperature, k_B – Boltzmann constant. The Vogel-Fulcher law usually manifests in disordered materials expecting a “freezing” of its dynamic at some finite temperature above 0 K such as relaxor compounds (see e.g. in [25]). Or for position of real or imaginary part maximum of complex dielectric permittivity:

$$v = v_o \exp\left(\frac{-E_a}{k_B\left(T_m - T_f\right)}\right) \tag{14}$$

where v_0 is the attempt frequency of dipole reorientation, E_a is the activation energy (i.e., the energy barrier between two equivalent polarization states), k_B is the Boltzmann’s constant, and T_f is the static freezing temperature

of the polarization fluctuations (i.e., the temperature below which dynamic reorientation of the dipolar cluster polarization can no longer be thermally activated), T_m – temperature of maximum permittivity at frequency ν. Note that the parameters obtained by fitting with Eq. (13) and Eq. (14) always will be different, except the Debye medium case [38].

Another important problem is the structure and the behaviour of polar nanoregions. The percolation of polar nanoregions was claimed to exist close to the freezing temperature [39] and in strong dc electric field close to the transition from relaxor to ferroelectric state [40]. However, the nature of such percolations of course should be different. A fractal structure of polar nanoregions was observed in typical relaxor PMN by means of broadband light scattering spectroscopy [41]. A fractal dimension in PMN at T<200 K was estimated - 2.61, in good agreement with that theoretically obtained in 3D space [41].

2.5. Size effects

There is an increasing interest in the studies of ferroelectric nanostructured ceramics as many devices are developed for microelectronic applications. Whereas for conventional ferroelectrics such as $BaTiO_3$ or $PbTiO_3$ the experimental situation begins to be well documented, the investigations on its nanostructured counterparts are still intense and in some cases contradictory [42]. The points of interest include the so-called size effect, i.e. the reduction of dielectric permittivity, spontaneous polarization, Curie temperature, piezoelectric properties with the decrease of size of the nanostructured materials [43]–[45]. Many theoretical models, including modified Landau-Ginzburg theory [44], effective medium theory [45], generalised brick-layer model [9] and others have been published in the last decades trying to explain the phenomena. It was shown that the extrinsic and intrinsic effects are of the great importance in explaining the reduction of dielectric permittivity,

spontaneous polarization, etc. For instance, it was shown that for nanosized $BaTiO_3$ capacitor the extrinsic contributions can be eliminated and the dielectric response remains typical for bulk single crystal [46]. On the other hand intrinsic effects, such as a change of local symmetry, a shift of soft mode frequency due the grain size effect can also be very important for ferroelectrics [47].

The influence of grain size on the dielectric properties of relaxors and mixed ferroelectrics close to the morphotropic phase boundary was studied mainly at low frequencies (i.e. below 1 MHz) [48]–[51]. It was established that the dielectric permittivity of PMN at low frequencies decreases with reducing grain size and the effect can be explained by a core-shell model [52] which assumes existence of a dead layer on the surface of the grains, and permittivity of the layer is much lower than of the grain itself. The model predicts a reduction of the maximum of the dielectric permittivity with decrease of the grain size due to grain boundary dilution. The dielectric anomaly typical for relaxors completely vanishes in PMN ceramics with 30 nm grain size [52]. The smeared dielectric response of nanograin ceramics was explained in [53] as the clamping of PNRs to the grain boundaries. In [51] these observations have been interpreted as the consequence of the continuous disappearance of the correlations between the PNRs that, in turn, gives rise to a transition from a relaxor (interacting PNRs) to a superparaelectric (independent PNRs) state. However, the dielectric investigations of grain size effect in a wide frequency range could be much more interesting. For example, it was established that in $PbMg_{⅓}Nb_{⅔}O_3$-$PbTiO_3$ (PMN-PT) with reduction of grain size the ferroelectric phase transition transforms into relaxor-like anomaly [53]. Moreover, the shift of dielectric anomaly in PMN with different grain sizes to lower temperatures was observed [54].

3. Experimental techniques

The main experimental technique used to obtain results presented in this thesis is broadband dielectric spectroscopy.

At low frequencies (20 Hz – 1 MHz) investigations were performed using Hewlett Packard 4284A precision LCR meter. Capacitance and loss tangent were measured. Silver paste was used as contact material on ceramic samples. Powders were measured using special sample holder.

Temperature was measured using 100 Ω platinum sensor and Keithley Integra 2700 multimeter. Temperature was varied with approximately 1 K/min rate.

Inductance and resistance of cables and silver contact is negligible at low frequencies, thus system was calibrated by capacitance measurement of empty system.

Dielectric permittivity was calculated using flat capacitor model :

$$\varepsilon' = \frac{(C_x - C_0)d}{\varepsilon_0 S} + 1, \qquad \varepsilon'' = \frac{\varepsilon'(C_x \mathrm{tg}(\delta_x) - C_0 \mathrm{tg}(\delta_0))}{C_x - C_0} \tag{15}$$

Here, C_x and $\mathrm{tg}(\delta_x)$ are capacitance and loss tangent of the system with the sample, C_0 ir $\mathrm{tg}(\delta_0)$ – capacitance and loss tangent of the empty system, ε_0 – electrical constant, d and S – height and contact area of the sample.

A vector network analyser Agilent 8714ET was used for measurements in 300 kHz – 3 GHz frequency range. The sample was connected as a termination of a coaxial line in this case. The analyser would measure reflection coefficient from the sample, which allows to calculate complex dielectric permittivity.

Similarly to low frequencies, temperature was measured using 100 Ω platinum sensor and Keithley Integra 2700 multimeter. Temperature was varied with approximately 1 K/min rate.

Calculation of dielectric permittivity is similar to the case of low frequencies (eq. (15)):

$$\varepsilon^* = \frac{(C_x^* - C_0^*)d}{\varepsilon_0 S} + 1 \tag{16}$$

Here, C_x^* and C_0^* are complex capacitances of the system with and without the sample. However, values are complex this time, as it greatly simplifies mathematical representation.

As it is known, reflection coefficient R^* depends on load connected to the transmission line:

$$R^* = \frac{Z - Z_0}{Z + Z_0} \tag{17}$$

Here, Z_0 is wave impedance of the transmission line, which is equal to 50 Ω in our case, and Z is impedance of the sample. If we denote Y^* as admittance of the sample, then

$$R^* = \frac{\frac{1}{Y^*} - Z_0}{\frac{1}{Y^*} + Z_0} \tag{18}$$

The vector analyser measures reflection coefficient only, and capacitance needs to be calculated as follows:

$$Y^* = \mathrm{j}\,\omega C^* = \frac{1}{Z_0}\frac{1 - R^*}{1 + R^*} \tag{19}$$

A different method needs to be applied in case of superhigh frequencies (3 – 40 GHz). In our case, three waveguide setups were available: 8 – 12 GHz, 27 – 37 GHz and 35 – 55 GHz. The sample would be in a shape of dielectric rod placed in the middle and perpendicular to the longer wall of the waveguide. TE_{10} mode was excited in the system. Absolute values of reflection and transmission coefficients were measured using Elmika R2400 scalar network analysers.

Temperature was measured using copper-constantan thermocouple and Keithley Integra 2700 multimeter. Temperature variation rate was kept around 1 K/min.

Dielectric rod inside the waveguide is an irregularity which scatters part

of radiation. Part of it is reflected, another part – passes through. Reflection and transmission coefficients depend on various system parameters, such as excitation mode, dimensions of the waveguide (only width of the longer wall a in case of TE_{10} mode), frequency of the electromagnetic wave v, complex dielectric permittivity of the sample ε^*, radius of the dielectric rod r. Complex dielectric permittivity can be found from a nonlinear equation $\varepsilon^* = f(R, T)$ or $\varepsilon^* = f(R^*)$ (here R^* and T^* are complex reflection and transmission coefficients, respectively).

However, in reality exact analytical expression of dielectric permittivity is not known for this case [55]. On the other hand, it is possible to solve optimisation problem in the form

$$\begin{aligned} R &= f_1(\varepsilon', \varepsilon''), \\ T &= f_2(\varepsilon', \varepsilon'') \end{aligned} \tag{20}$$

Optimisation procedure can be stopped when

$$\left|R - f_1(\varepsilon', \varepsilon'') < \delta\right| \text{ and } \left|T - f_2(\varepsilon', \varepsilon'') < \delta\right| \tag{21}$$

Here, δ – calculation precision. Values of dielectric permittivities are obtained when the inequalities (21) are satisfied.

4. Experimental results: Relaxors

4.1. Dielectric investigations of $PbMg_{1/3}Nb_{2/3}O_3$ powders

$PbMg_{1/3}Nb_{2/3}O_3$ (also known as PMN) is perovskite material and is known as a canonical relaxor as it is one of the first ever created and is highly investigated [21], [56], [57]. It has a broad anomaly around 270 K with dielectric permittivity around 10000, with contribution of polar modes being relatively small. It does not exhibit any spontaneous phase transitions, and its freezing temperature from mean relaxation time is around 225 K.

4.1.1 Experimental results

Powders with various grain sizes in the range of 15 nm to 1000 nm were obtained by annealing a PMN nanopowder (15 nm) at increasing temperature between 650 °C and 1200 °C for 30 min. The starting nanopowder was prepared by direct mechanical activation of PbO (Aldrich, 99.9% + >10 μm) and columbite $MgNb_20_6$ (Alfa Aesar 99.9%). The synthesis was carried out in air using a Retsch mill PM 100 specially equipped for mechanical alloying working at 450 rpm. Typically 12h was necessary to obtain pure perovskite phase of PMN from the starting oxides. Extensive scanning electron microscopy, transmission electron microscopy, atomic force microscopy, and X-ray characterisations were performed, in particular to check the quality, the morphology and to measure the grain size distribution. In each case, samples with narrow Gaussian size distribution were chosen for the measurements

The dielectric properties of various mean grain sizes of PMN powders (15 nm, 30 nm, 40 nm, 65 nm and 150 nm) have been investigated only in the low frequency range (20 Hz – 1 MHz with HP 4284A LCR meter) because of the difficulties to put them into coaxial line. Powders have been put into teflon cylinder with cylindrical cavity inside and the copper contacts have been

applied from top and bottom with the small pressure just to achieve a good electrical contact. The influence of teflon cylinder on the dielectric response of the system has been separated by the prior measurement of cylinder with the air gap inside and a subsequent subtraction of this data from the total dielectric permittivity for each data point. All powders have been annealed at 400 K to remove water vapour and the measurements have been performed during cooling cycle down to 110 K.

The temperature and frequency dependencies of the real part of dielectric permittivity of PMN powders with a few selected grain sizes (15 nm 40 nm and 150 nm [58]) are presented in figure 4.1.1. The dielectric permittivity values were normalised to maximum permittivity obtained for each specimen due to impossibility to determine the powder-to-air ratio in the specimen. As it is seen from figure 4.1.1, the dispersion occurs below room temperature, thus, to highlight the dispersion region, we show the temperature dependences only

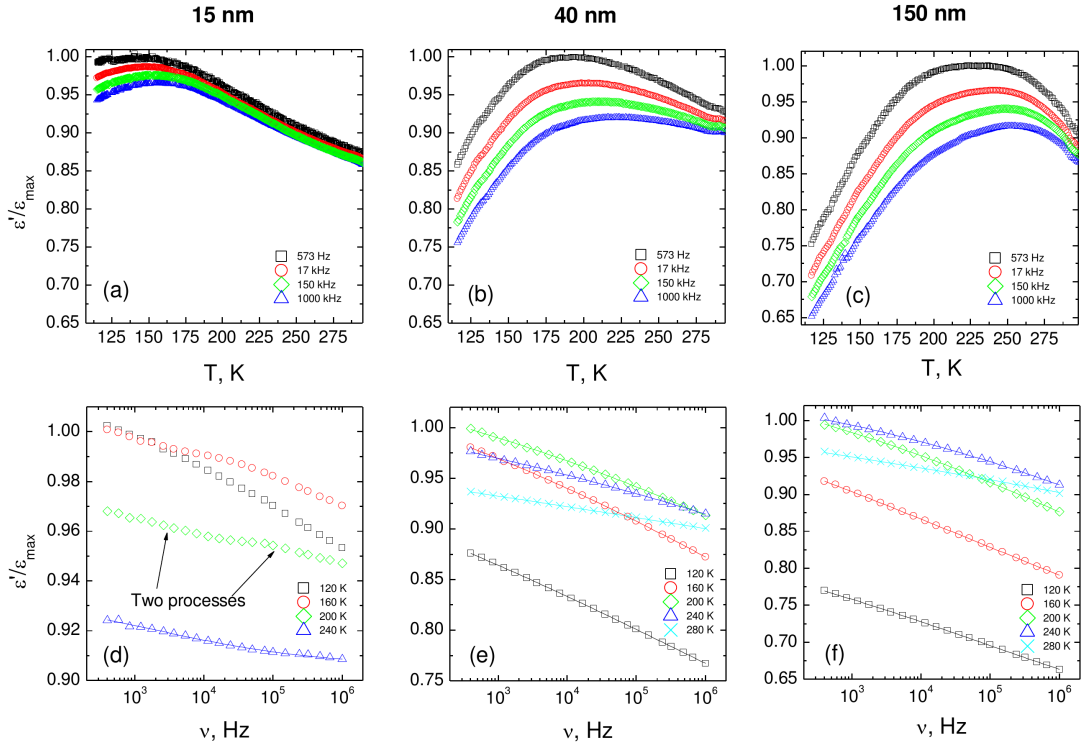

Figure 4.1.1. Temperature (a, b and c) and frequency (d, e and f) dependences of the real part of normalised dielectric permittivity of PMN powders with different grain sizes. Solid lines in frequency dependences represent Cole-Cole fits.

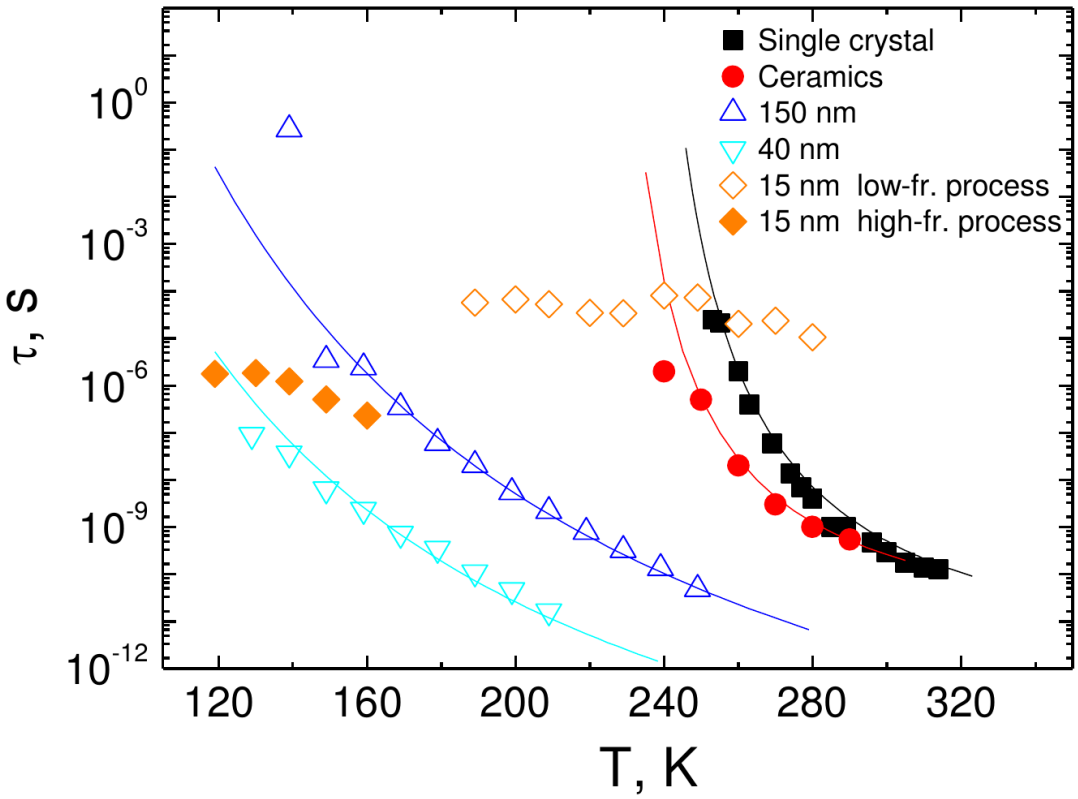

Figure 4.1.2. Temperature and grain size dependence of the mean relaxation time obtained from Cole-Cole formula for PMN powders. Solid lines represent Vogel-Fulcher fits.

below 300 K. Two main features of dielectric behaviour can be indicated. First, a remarkable shift of the dispersion region to the higher temperatures with the grain size increase (figure 4.1.1 (a), (b), (c)) is observed. Second, a reduction of the dielectric dispersion on the decrease of the grain size of powders is also clearly visible, especially if one compares 150 nm [58] and 15 nm curves (figure 4.1.1 (a) and (c)). To go into a deeper analysis the dielectric data in frequency domain are presented. The frequency dependencies of dielectric permittivity (figure 4.1.1 (d), (e) and (f)) show a substantial dispersion in all investigated frequency range.

The experimental data was approximated with conventional Cole- Cole formula (3). The fit lines are in a good agreement with experimental data (figure 4.1.1). The analysis of the data revealed that the dielectric dispersion

broadens upon cooling, especially below 200 K, and shifts to lower frequencies. These frequency dependences are much broader than the usual Debye type dispersion, except for the smallest (15 nm) grain size powders. Two overlapping relaxational processes were observed in the former case at temperatures below 200K, therefore a superposition of two Cole-Cole processes has been used in the fitting procedure. The mean relaxation time obtained from the Cole-Cole fits (figure 4.1.2) has been analysed in terms of Vogel-Fulcher law (13).

The Vogel-Fulcher law usually manifests in disordered materials expecting a “freezing” of its dynamic at some finite temperature above 0 K such as relaxor compounds (see e.g. in [25]). Good approximation of the data (solid lines in figure 4.1.2) has been obtained for all grain size powders except for the smallest ones, for which almost no temperature dependence of τ is observed, in agreement with previous observation of disappearance of relaxor character at smallest grain sizes [48].

To find out the influence of the mean grain size to the properties of PMN powders the temperature of the maximum dielectric permittivity, T_{max}, and the values of freezing temperature T_0 versus grain size are presented in figure 4.1.3. Here the experimental points for PMN ceramics, single crystal and 150 nm powders, taken from our earlier investigations [58]–[61] have been added for comparison. All these data behave coherently: from micrometric sizes T_{max} decreases smoothly with reducing grain size, however, an abrupt decrease of T_{max} occurs below 60 nm. The evolution is similar to the grain size dependence of the Curie temperature obtained for $BaTiO_3$ [62] or $PbTiO_3$ [63] perovskites despite the fact that no ferroelectric phase transition takes place in PMN without a bias electric field [64].

Grain size dependence of the freezing temperature is very similar. The T_0 is almost grain size independent if grains are bigger than ~300 nm. However, an abrupt decrease of the freezing temperature occurs with reducing grain size from 300 nm to 40 nm. Finally, freezing temperature reaches zero in PMN

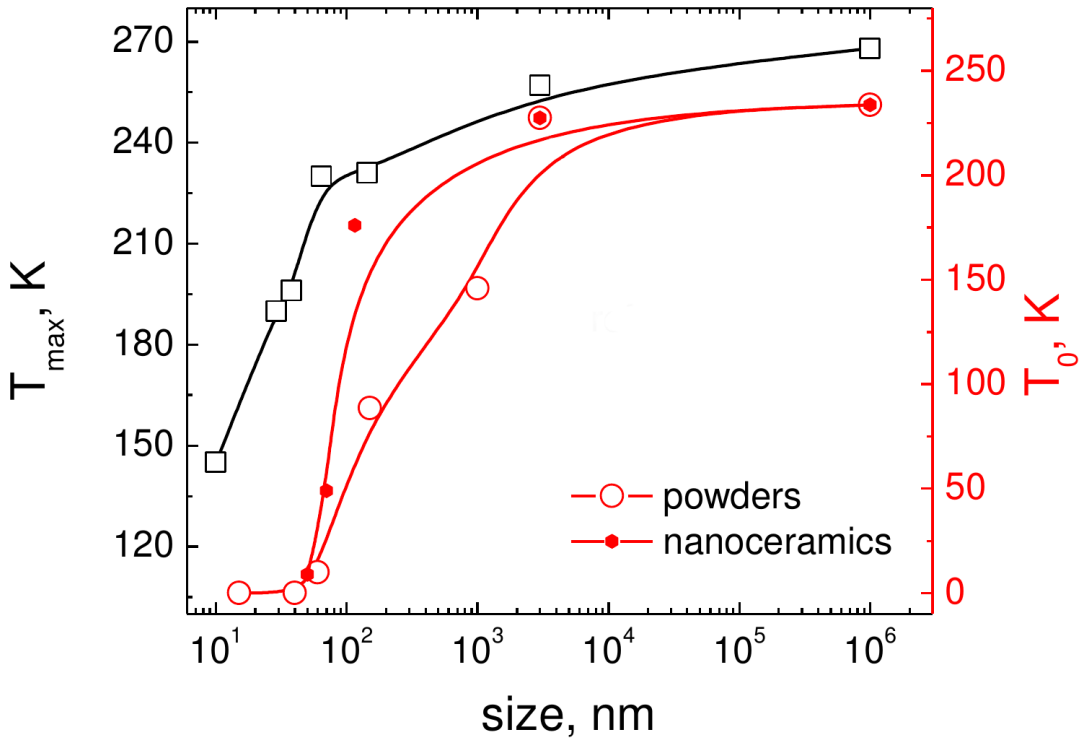

Figure 4.1.3. Grain size evolution of T_{max} at 1 kHz frequency (black squares) in PMN powder samples and dipole freezing temperatures obtained from Vogel-Fulcher fits for PMN powders (red open circles) and nanograin ceramics (red filled hexagons). The two rightmost points are taken from refs [59], [60]. Data for ceramics is taken from [61]. Solid lines are guidelines for eyes.

powders with grain sizes smaller than 40 nm.

4.1.2 Comparison of powders and ceramics

A thorough study of nanostructured PMN ceramics was presented in [61]. Here, we will compare the presented properties of PMN powders with properties of ceramics presented in [61].

Several similarities can be noticed between properties of powders (presented here) and ceramics. First of all, dielectric investigations of both powders and ceramics show, that the Vogel-Fulcher law describes temperature evolution of dynamic properties of the material related to polar nanoregions. In this respect, our data correlates well with results for bulk PMN [59], [60].

Secondly, the bigger the grains, the higher the freezing temperature derived from Vogel-Fulcher law. According to high resolution X-ray investigations of micrometer PMN the correlation length associated with mean size of PNRs is higher than 40 nm below 200 K [65]. In contrast, in nanometric samples it is limited by the grain size [48]. On the other hand, the Vogel-Fulcher law is well known to be a manifestation of cooperative interaction of some type of entities (PNRs in case of relaxors) [66]. Grain boundaries can be expected to limit interaction between PNRs in different grains. In that case, the smaller the grain size, the smaller correlation length between the PNRs are. This means that freezing temperature is expected to be lower in case of smaller grains, and would vanish in case of very small grains. This is exactly what we observe, with critical grain size of 40 nm. In case of smaller grains no freezing (glass behavior) is observed in both dielectric and NMR measurements presented in [61].

Another important observation is that temperature of the maximum of dielectric permittivity T_{max} shifts to the higher values with increase of grain size in both powders and ceramics. This could be related to the fact that in case of powders relaxation time is proportional to the grain size. It is unknown if static permittivity of relaxors has a peak, as it is expected to be observable at infinitely low frequencies at low temperatures [67]. The peak observed at a fixed frequency is due to the fact that the static permittivity increases on cooling (figure 4.1.1), but the mean time also increases according to the Vogel-Fulcher law (figure 4.1.2). A selected relaxation time is observed at higher temperatures in bigger grains in case of powders, thus T_{max} increases. However, this observation is only weakly valid for higher frequencies in case of ceramics, and at lower frequencies the trend is opposite – the bigger the grains, the smaller T_{max}. These effects can be explained by the fact that in case of ceramics distribution of short relaxation times is nearly unaffected by grain size, while long relaxation times are suppressed in smaller grains due to absence of big PNRs. As a result, a more pronounced dispersion of dielectric

permittivity is observed in bigger grains, and T_{max} shifts to higher temperatures. However, it remains unclear, why relaxation time is proportional to grain size in powders, and why short relaxation times are nearly grain size-independent in ceramics. Probably, some kind of interaction between grains exists in ceramics, which is absolutely absent in powders. This interaction could be related to strain, as dipolar interactions should be of shorter range and are thus a less likely mechanism. This mechanism could be a subject of a separate investigation.

The dielectric properties of smallest (15 nm) grain size PMN powders are rather unusual compared to the other ones. Here we see two weak relaxational processes which is not the case in coarse-grained PMN powders where only one process is observed in the dielectric spectra. To explain this nuclear magnetic resonance (NMR) measurements of ^{93}Nb were performed in [61]. It was shown that the behaviour of a spin-lattice relaxation time is two-component one. The latter fact could mean that one of the NMR-active processes is related to non-polar mechanism (e.g. grain boundaries). However it is easier to explain the data by assuming that there are 3 processes involved. It is most likely, that in smaller grains a process, which determines dielectric properties, diminishes. As a result the NMR-related processes are not obscured anymore. They probably are present in dielectric properties of coarse-grained ceramics, too, but overshadowed by the main relaxational process, which is responsible for relaxor properties of the material.

4.2. Nanostructured $PbSc_{½}Nb_{½}O_3$ ceramics.

Relaxor ferroelectric $PbSc_{½}Nb_{½}O_3$ (PSN) is one of the classic relaxor materials. Its main difference from other canonical relaxors like PMN is presence of a spontaneous first-order phase transition from relaxor to ferroelectric state at 367 K temperature during zero-field cooling cycle [68]. The situation is not unique, similar properties are exhibited by other materials,

like a very similar $PbSc_{½}Ta_{½}O_3$ (PST) [27] or much more complicated ternary solid solutions [69]. PSN (as well as PST) has several important properties. B-site ions could be ordered or completely disordered or have any type of ordering in between. A spontaneous ferroelectric phase transition occurs in case of complete ordering without any relaxor behaviour. The latter is exhibited only in case of B-site disorder, although the spontaneous phase transition still takes place if the compound is stoichiometric and no lead vacancies are introduced. Thus size effects in stoichiometric disordered PSN ceramics might be different from both classic relaxors and classic ferroelectrics.

The first study of nanostructured disordered PSN was reported in [70]. It contained studies with X-ray and dielectric spectroscopy in 1 – 1000 kHz range, mainly focused on structural data. It was reported that structure of the samples is actually a mixture of rhombohedral R3m and monoclinic Pm structures at 85 K temperature. Structure is predominantly (but not pure) rhombohedral at big grain sizes and monoclinic at small ones with an almost step-like change of structure concentration at around 65 nm, which cannot be explained by a different crystal structure at the surface of the grains. At high temperatures the ceramics are reported to be cubic $Pm\bar{3}m$ independently of grain size. This fact is important for 2 reasons – firstly, this implies that variation of grain size modifies mechanism of phase transition resulting in a discontinuous change in ground-state symmetry. Furthermore, the presence of phase transition means that the compound is stoichiometric, as phase transition is expected to be suppressed otherwise [68]. Moreover, it was found that crystal lattice becomes increasingly strained when grain size is reduced below critical size, which is accompanied by increase of polarization estimated from Rietvield refinement.

Later some of the samples studied in [70] were investigated by the author of the thesis by means of broadband dielectric spectroscopy in 100 Hz – 55 GHz frequency range [71]. The grain sizes were 20, 40 and 80 nm, which are

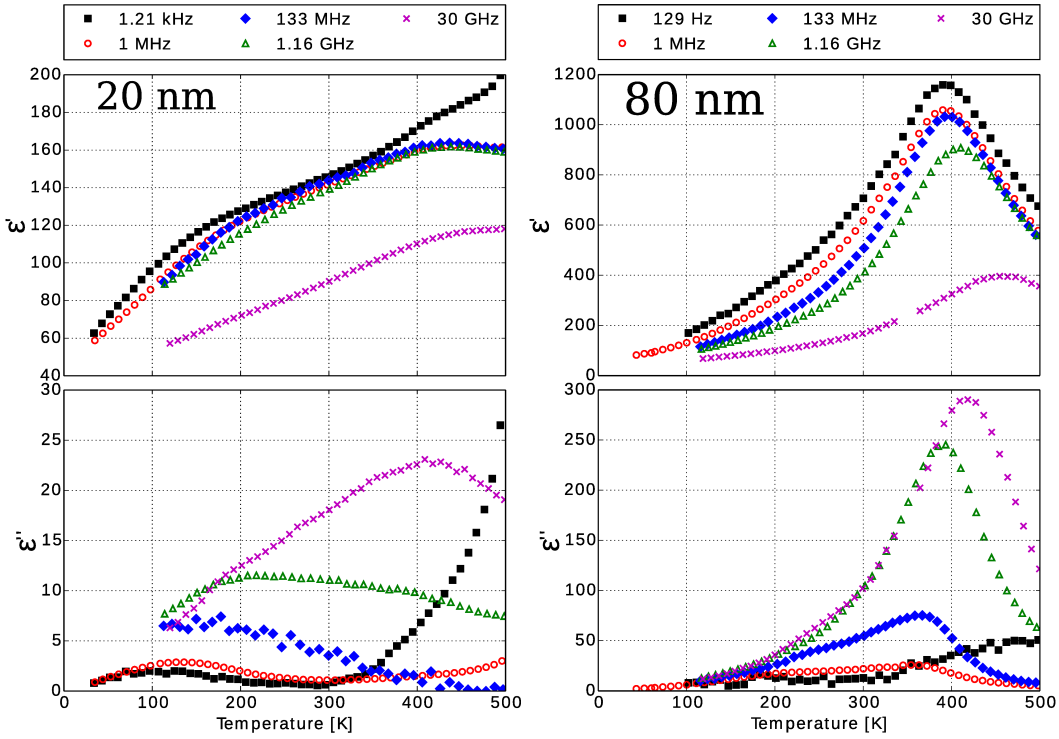

Figure 4.2.1. Temperature dependences of the real (top) and imaginary (bottom) parts of complex dielectric permittivity of 20 nm (left) and 80 nm (right) grain size PSN ceramics. Data taken from [71].

around the previously reported critical size of 65 nm. Temperature dependences of the dielectric permittivity of 20 nm and 80 nm ceramics are presented in figure 4.2.1. There are several important differences from bulk ceramics. Firstly, dielectric anomaly around 400 K is suppressed. This could be qualitatively explained by the venerable coated spheres. The smaller the grains, the smaller the permittivity. However, a spontaneous phase transition is invisible and the ceramics exhibit purely relaxor-like properties. Similar effect had previously been observed in PMN-35%PT [53]. In the latter case the phase transition was observed in coarse grained (4 μm) ceramics which were made from the same starting powder as fine grain (150 nm) ones. Absence of the transition was explained by existence of grain boundaries, which would limit percolation of polar nano regions (PNRs). Furthermore, only low frequency process assigned to flipping of the PNRs was influenced by grain size, while

high-frequency processes were mostly unaffected. Only small broadening and suppression of dielectric anomaly of PMN-PT was observed at 250 GHz [53]. In PSN both substantial broadening and suppression of the anomaly were observed at 30 GHz (figure 4.2.1). This could be due to several reasons. Firstly, lower frequencies are compared in PSN. Secondly, grain sizes were much bigger in case of PMN-PT. Nonetheless, both suppression of percolation and smearing of the anomaly should be taken into account to explain the observed effects in PSN. Moreover, X-ray studies clearly showed presence of structural phase transition [70]. This means that in reality grain size does not suppress the transition itself, but dielectric anomaly is mostly influenced by other processes (like contribution of PNRs or domain walls in ferroelectric state). Presence of grain boundaries suppresses these contributions, which, in turn, influence crystal symmetry of ferroelectric state.

Another important feature of dielectric spectra of PSN is low-temperature relaxation. To the best of our knowledge it has been mostly ignored previously, as the process is very faint at low frequencies and is obscured by the main anomaly, but it is very nicely seen in 20 nm ceramics (figure 4.2.1). The process takes place at low temperatures (below 200 K even at 1 GHz), making analysis of its dynamics very difficult. The actual mechanism of this process is obscure, as very little data is available. It could be related to some type of disorder in the material, e.g. second relaxor-like process or coexistence of dipolar glass and ferroelectric states similar to $(Rb,NH_4)H_2AsO_4$ (RADA) crystals [72]. Another possible mechanism is contribution of ferroelectric domains, whose relaxation time usually follows Arrhenius law (see e.g. $BaTiO_3$ in [73]) with some exceptions (i.e. KDP family) without a proper explanation (see e.g. [16], [74]). Similar behavior has also been previously observed in other relaxor materials with a spontaneous ferroelectric phase transition [69].

Additional information becomes available when temperature dependences of dielectric permittivity of ceramics with different grain sizes at a selected frequency are compared. In figure 4.2.2 we can see that reduction of grain size

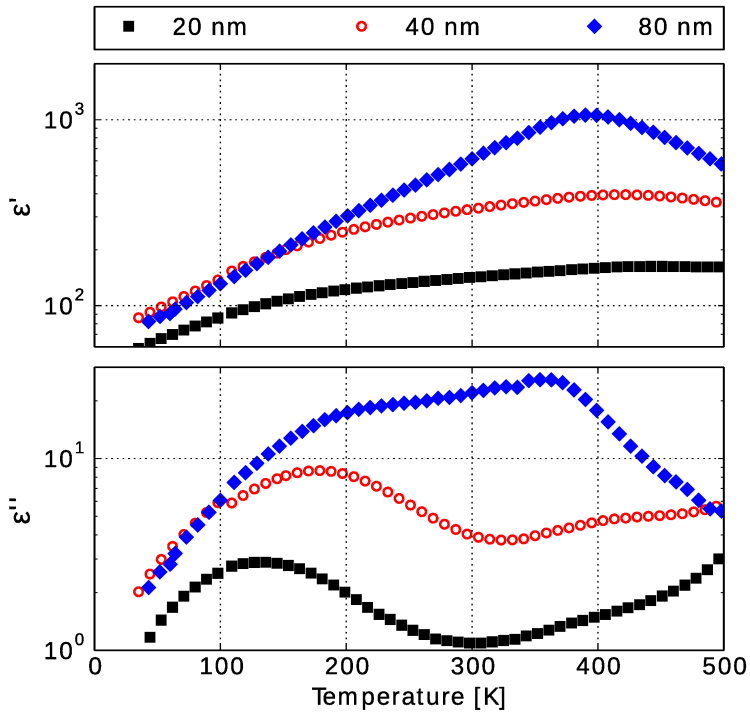

Figure 4.2.2. Temperature dependences of the real (top) and imaginary (bottom) parts of complex dielectric permittivity of PSN ceramics with different grain sizes at 1 MHz.

suppresses the anomaly around 400 K, and its temperature is actually shifted to higher temperatures. The shift cannot be explained by rise of electrical conductivity at smaller grain sizes, for example, as from fig. 4.2.1 we can see that dispersion at 1 MHz in finest ceramics is virtually non-existent. Moreover, the values of dielectric permittivity tend to become very similar at low temperatures, although finest ceramics exhibit somewhat smaller permittivity. The latter fact could be explained by potentially smaller density of the sample and high strain of the lattice as reported from X-ray studies [70].

From evolution of dielectric losses in figure 4.2.2 we can see that low temperature process is shifted to lower temperatures when grain size is reduced, with dielectric losses becoming smaller. Another important fact is that dielectric losses related to anomaly around 400 K are reduced much faster than dielectric permittivity itself. Moreover, losses in 80 nm ceramics are bigger at

400 K than at low-temperature process, but it is vice versa in 20 nm ceramics.

The biggest problem is to explain all of these observations. Shift of the low-temperature process to lower temperatures with reduction of grain size could be explained if we assume that this process is related to either PNRs or dipolar glass-like regions in otherwise ferroelectric matrix. In that case the same train of thought as used to explain size effects in PMN can be used. Interactions between the polar entities would be limited at smaller grain sizes. Besides, average sizes of these regions would be smaller. This means that entities with a much lower volume (and mass) are moved by electric field in smaller grains, which would make associated relaxation times shorter. Another possible (and equivalent) interpretation is suppression of long relaxation times by surfaces of the grains. On the other hand, relaxation times would still increase upon cooling. However, the same relaxation time would be achieved at lower temperatures in ceramics with smaller grains. This would manifest itself as a shift of anomaly to lower temperatures upon reduction of grain size. The material itself is a relaxor (albeit with a phase transition), thus it is most likely that we have PNRs and not dipolar glass-like regions. In that case the shift of this anomaly would have the very same mechanism as in case of shift of T_{max} in PMN powders or in case of high frequencies in ceramics.

It is also possible to assume that the shift of anomaly is related to EMA effects. In core-shell structure, the smaller the grains are, the shorter is the relaxation time in case of grain boundary medium having a smaller dielectric constant [75]. However, the effect would be visible only if there is a big difference in grain size, which we don't have in this case. This supports idea of PNR-related effects.

The anomaly around 400 K is also suppressed, but in a little different manner. The behavior is very similar to PMN ceramics at low temperatures – the smaller the grain, the higher the T_{max}. It is very likely that the mechanism in this case is also very similar. We can assume that contribution of very small PNRs and polar phonons is unaffected by grain size and their contribution has

a maximum at temperatures slightly higher than 400 K. Then in case of coarse-grained ceramics flipping of PNRs, which happens with long relaxation times, would produce an anomaly at a little lower temperatures, just above the spontaneous phase transition. However, if the flipping of the big PNRs (or their existence) is suppressed, this would be manifested in an apparent shift of the anomaly. It is possible, however, that the temperature of the phase transition is not shifted in reality.

4.3. Summary

In summary, very complex size effects on dielectric properties of PMN powders and PSN ceramics were observed. Evolution of the dielectric properties could be explained by core-shell structure of the grains approximately. However, this model alone is insufficient and modification of bulk properties by grain size must also be taken into account. Grain boundaries limit growth and interactions of PNRs, which is very important for freezing temperature and relaxation times of PNRs. However, interactions between adjacent grains are probably still present in ceramics.

PNRs are playing a key role in determining dielectric properties of relaxors. On the other hand, the spontaneous phase transition in PSN ceramics is not driven by PNRs alone, as suppression of the anomaly leads to a modification of ground state, but the phase transition is not eliminated.

5. Experimental results: $0.36BiScO_3$-$0.64PbTiO_3$

Piezoelectric materials are highly important for our everyday lives, with many of them being ferroelectric [76]–[78]. Bi*Me*O_3-$PbTiO_3$ (Me^{3+} is a cation with octahedral coordination) solid solutions are known to have high Curie temperatures. Specifically, (1-x)$BiScO_3$-x$PbTiO_3$ (BS-PT) solid solutions exhibit a morphotropic phase boundary around x=0.64 with transition temperature around 450 °C [79]. This is 100 ºC above that of Pb(Zr,Ti)O_3.

Investigations of piezoelectric and ferroelectric properties of $BiScO_3$-$PbTiO_3$ have been previously reported in a number of papers [80]–[83]. It is known that upon decrease of grain size dielectric permittivity around room temperature decreases, and coercive field increases to the point when ferroelectric loops become impossible to observe. The coercive field increases and remanent polarization decreases. Although macroscopically absent, the loops are still visible with piezoelectric force microscopy technique even in nanocrystalline ceramics. The observed change is due to grain boundaries, which screen the electric field within the grains and makes switching difficult in the case of nanoscale grains. The boundaries also dominate impedance in the latter case. Furthermore, a shift of Curie temperature down to 400 °C is observed.

Broadband dielectric investigations of BS-PT ceramics were previously reported in [84], and some questions were rose then. Firstly it was not understood where the relaxor-like dispersion observable below room temperature comes from. It has been associated either to contribution of domain walls or to some kind of fractal-like entities inside the ferroelectric matrix, possibly polar nanoregions not unlike the ones in classical relaxors. Secondly, a high-frequency process was observed and it was related to domain wall movement and electromechanical coupling, with domain thickness being the factor determining the characteristic wavelength of the process.

5.1. Broadband dielectric properties

Temperature dependencies of dielectric properties of the ceramics with different mean grain sizes are presented in figure 5.1.1. Measurements were performed in the ferroelectric phase only, so the dielectric anomaly associated with the ferroelectric transition is not visible. Dielectric properties of coarse grained ceramics were reported elsewhere in a limited frequency range [81], with anomaly taking place around 470 °C. Broadband properties of the coarse-grained ceramics are also in agreement with previous results reported in [84], where data was reported in broader temperature and frequency ranges. Both here and in previous reports conductivity is the main mechanism driving dielectric losses at frequencies below 300 Hz and temperatures above 450 K. In both cases a relaxor-like anomaly is observed below 300 K, which manifests in nearly frequency-independent losses below 200 K and peaks in imaginary part which shift to higher temperatures when frequency is increased.

The nanograined ceramics are made from the same starting materials, but its low-frequency permittivity saturates at 900 above 300 K. The dielectric anomaly in the vicinity of phase transition is known to be nearly invisible in this case [81]. On the other hand, both nanograined ceramics and the ceramics investigated in [84] show very nice relaxor-like peaks in imaginary part of the dielectric permittivity, while coarse-grained ceramics in our case exhibit very broad peaks, which overlap with charge relaxation-related process. The reason for the difference between the coarse-grained ceramics studied here and those of [84] could be related to the different processing. The starting powder for the ceramics in [84] was produced by conventional means (involving milling with zirconia balls) [85]. In our case the powders were produced by mechanosynthesis using tungsten carbide (WC) as the milling media. This means that different doping and/or defects might potentially be introduced into the system, which might alter relaxational dynamics. The distribution of relaxation times might be broadened, or temperature dependence of the mean

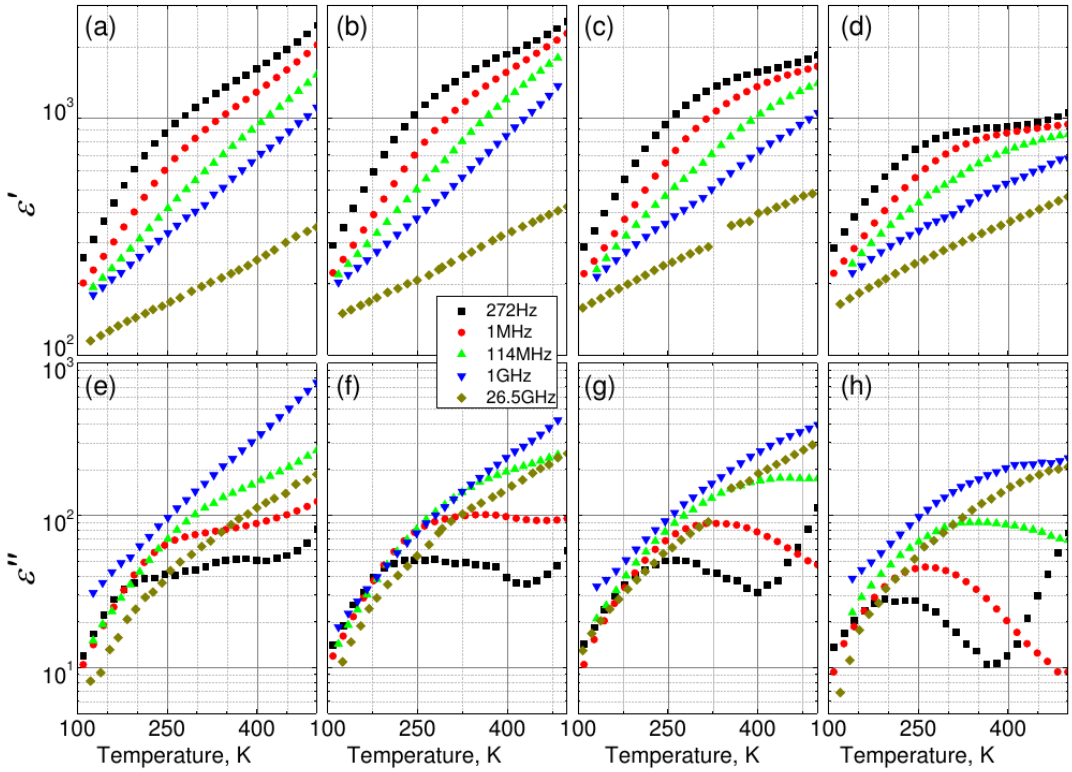

Figure 5.1.1. Temperature dependences of the real ((a), (b), (c) and (d)) and imaginary ((e), (f), (g) and (h)) parts of dielectric permittivity of ceramics with mean grain size 1.6 μm ((a) and (e)), 200 nm ((b) and (f)), 50 nm ((c) and (g)) and 26 nm ((d) and (h)).

relaxation time might be altered, or both. On the other hand, the ceramics in our case are known to have very low doping level (W content as low as 550 ppm). However, a high level of residual microcrystalline strain was found, which is known to ony partially relax during processing [82]. This means that probably not the doping, but mechanical stresses make the difference. The fact that smaller-grained ceramics exhibit lower permittivity is not related to differences in processing, though. Evolution of the dielectric permittivity and visibility of the relaxor-like process as a function of grain size can be seen in figure 5.1.2. Here we can see, that at 11 kHz the smaller the grains, the narrower relaxor-like peaks of imaginary part are. This also makes them better visible. On the other hand, both real and imaginary part have a tendency to be

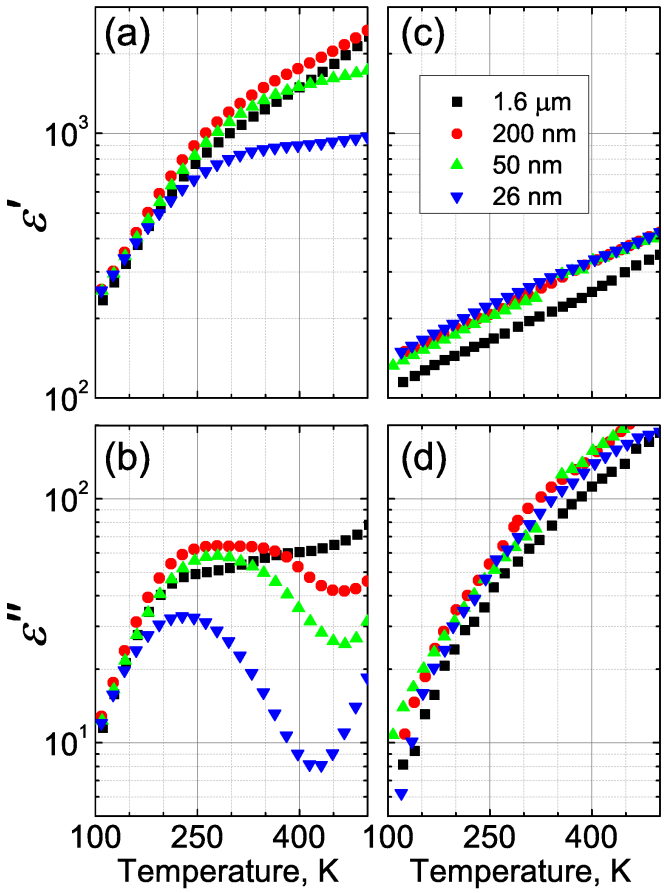

Figure 5.1.2. Temperature dependences of the real ((a) and(c)) and imaginary ((b) and (d)) parts of dielectric permittivity of ceramics at 11 kHz ((a) and (b)) and 26 GHz ((c) and (d)).

lower at smaller grains. The only exception here is coarse-grained ceramics, which have slightly smaller permittivity. On the other hand, all ceramics have the same complex permittivity at temperatures below 150 K. The latter fact virtually eliminates possibilities of poor quality of ceramics or error in measurements. This means that grain-size dependence of dielectric permittivity is non-monotonous at low frequencies at temperatures above 250 K. Similar behaviour was seen at room temperature in barium titanate ceramics [86]–[88], and it is likely related to contribution of domain walls [89]–[91]. The only difference from BTO is that its permittivity is maximum when grains are around 1 µm size, and in case of BSPT the maximum is observed between 50

nm and 1.6 µm.

Even though the ceramics are different at low frequencies, they cannot be distinguished at microwave frequencies. Coarse-grained ceramics have a slightly smaller permittivity compared to others, though. A very similar situation was observed in PMN-35PT [53]. This means that the main grain size-dependent process is inherently a low-frequency process.

The main reason responsible for size-dependence of dielectric permittivity in ferroelectric nanostructured ceramics is the formation of a dead layer on the grains of the ceramics (grain boundaries) [86], [92]–[94]. The dead layer is reported to be around 1 nm thick and its dielectric permittivity around 100 in $BaTiO_3$ [86]. This means that the dead layer influences properties of the ceramics only if the bulk of the grains has very high permittivity compared to the dead layer and/or if the volume of the layer is big enough. The latter means that the effect is only relevant in case of small grains, and can be ignored in case of coarse-grained ceramics. Properties of the coarse-grained ceramics can be assumed to be the same as the bulk properties of the material. Here we can also see that dielectric permittivity decreases around 5 times from around 1000 at 11 kHz to 200 at 26 GHz and 300 K in 1.6µm ceramics. If we assume the same properties of the dead layer in case of BSPT and apply a model of coated spheres [75] or the one of brick wall [7], we can see that the grain boundary would only be important at low frequencies, since there is a big difference in properties of core and shell (or brick and inter-brick medium). This is absolutely irrelevant at high frequencies, as properties of the grains are very similar to those of the grain boundaries, thus no size-effect (or grain boundary dilution) is observed. This also means that there is a relaxational process which is responsible for high permittivity of the bulk material at low frequencies. On the other hand, all the ceramics exhibit the same properties at 11 kHz at temperatures below 150 K. Again, the size effect vanishes. This could only happen if the low-frequency process vanishes, too. This could happen in two ways. Firstly, contribution of the process could diminish. The second possible

explanation is shift of the mean relaxation time to very long values. In the latter case 11 kHz would actually become “high frequencies”. We can see a relaxor-like behaviour, which always goes with a relaxation, at the relevant temperature range. Thus the low-frequency process responsible for the high permittivity is the same that gives relaxor-like anomaly.

There is a small detail regarding dielectric properties at 26 GHz. We can see from figure 5.1.2 that both dielectric permittivity and losses of coarse-grained ceramics are smaller than in other cases. The difference cannot be explained by experimental errors alone. This means that the real situation is slightly more complicated than simple grain-boundary dilution. We will come back to this point later on.

Frequency dependences of dielectric permittivity of BSPT ceramics at various temperatures are presented in figure 5.1.3. Experimental data was approximated by fits, represented with solid lines. Superposition of several Cole-Cole type processes was used as the approximation function (22).

$$\varepsilon(\omega) = \varepsilon_\infty + \sum_{k=1}^{N} \frac{\Delta\varepsilon_k}{1 + (\mathrm{i}\omega\tau_k)^{1-\alpha_k}} \qquad (22)$$

Here, N is the total amount of processes used, and it was equal to 3 in coarse-grained ceramics and 2 in all the others. ε_∞ is contribution of all polar processes at higher frequencies than available in this study, which include electronic and ionic polarizations. $\Delta\varepsilon_k$ is strength of the k-th process, τ_k is its mean relaxation time, and α_k is related to distribution of relaxation times [3]. The bigger the latter parameter is, the broader are the distribution of relaxation times and dispersion regions associated with the process. Angular frequency is denoted by ω and i is the imaginary unit.

The first process is a low-frequency process, which is visible at elevated temperatures. We assign it to Maxwell-Wagner type of polarization (charge separation). It was impossible to characterise it properly, as the current experimental data does not contain enough information about it due to limited

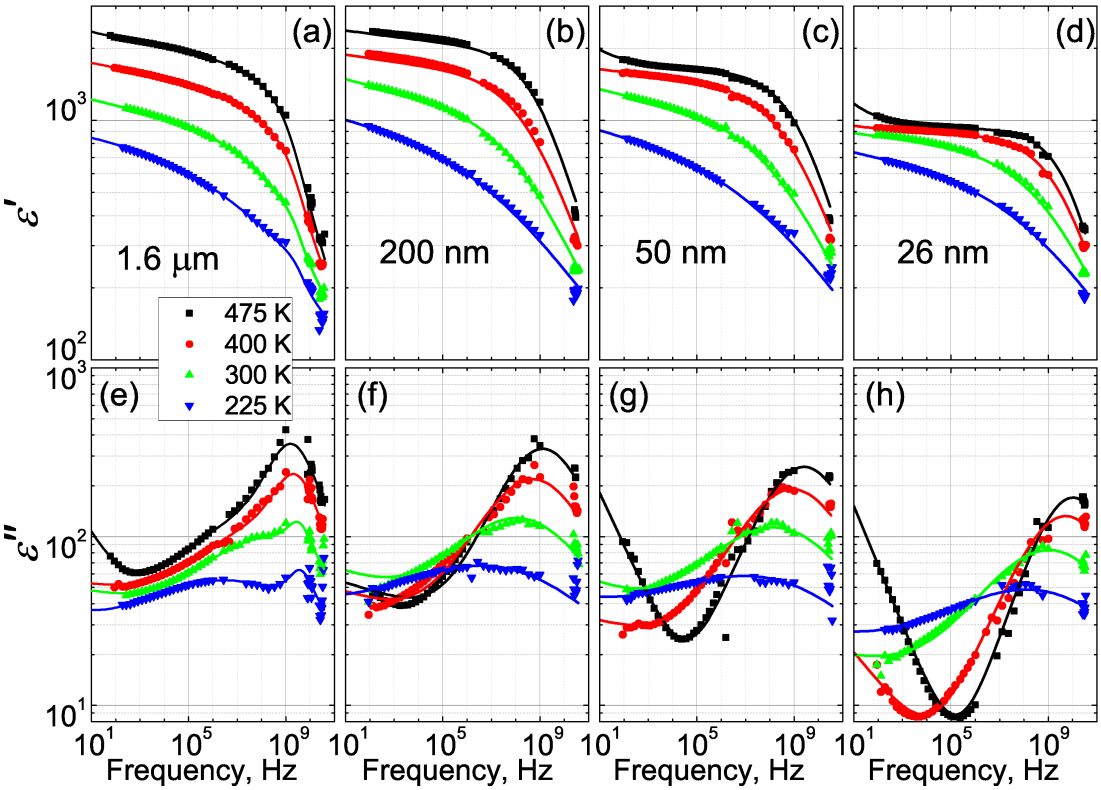

Figure 5.1.3. Frequency dependences of the real ((a), (b), (c) and (d)) and imaginary ((e), (f), (g) and (h)) parts of dielectric permittivity of ceramics with mean grain size 1.6 µm ((a) and (e)), 200 nm ((b) and (f)), 50 nm ((c) and (g)) and 26 nm ((d) and (h)).

temperature and frequency ranges. However, it was needed to include it in the fit to have reliable fits of other processes.

Another distinctive feature of the spectra is a broad process in 1 kHz – 1 GHz frequency range (the second process). Its both mean relaxation time and breadth of the relaxation region increase upon cooling. This second process is the one which is observed as relaxor-like process in temperature dependences and gives the biggest contribution to the low-frequency value of dielectric permittivity. It was previously assigned to be either contribution of domain walls or some fractal-type structural clusters inside domains, possibly polar nanoregions [84]. Thus it becomes interesting to analyse temperature evolution of the mean relaxation time of the process along with breadth of the dispersion

region. Top graph in figure 5.1.4 contains temperature dependence of α parameter of this process. The closer it comes to unity, the broader it becomes. The distribution becomes infinitely broad (constant loss regime) in the limit of $\alpha \rightarrow 1$. As we can see, this limit is approached upon cooling. This is observed for all materials with decreasing grain size down to the nanoscale, and the breadth of distribution of relaxation times is independent of grain size.

The bottom graph of figure 5.1.4 shows temperature dependences of the mean relaxation time of the second process. If the process would be a contribution from ferroelectric domains, then one would normally expect dependences following Arrhenius law like in BTO [15], as domain wall motion is thermally activated in ferroelectric materials. However, in our case Vogel-Fulcher dependence (equation (13)) is observed. This kind of behaviour is usually regarded as an evidence of a collective process (e.g. [66]), and is a characteristic of dipolar glasses (e.g. [95], [96]) and ferroelectric relaxors (e.g. [21], [56]).

Table 5.1.1. Dependence of activation energies, freezing temperatures and natural logarithm with corresponding expected values of attempt time of the second process on grain size.

Grain size (nm)	E_A (meV)	T_0 (K)	ln(τ_0/s)	τ_0 (ps)
1600	94 ± 20	107 ± 12	-26.4±1.3	3.4
200	37 ± 4	144 ± 3	-23.6±0.3	54
50	55 ± 8	99 ± 9	-24.1±0.4	34
26	93 ± 15	52 ± 15	-27.3±0.4	1.4

Activation energies, freezing temperatures and attempt times of the second process in various ceramics are presented in table 5.1.1. One can note a loose correlation between dielectric permittivity at room temperature, the freezing temperatures, the activation energies and the attempt time. Of the two ceramics with similar grain sizes (e.g. 1.6 μm compared to 200 nm, but not to

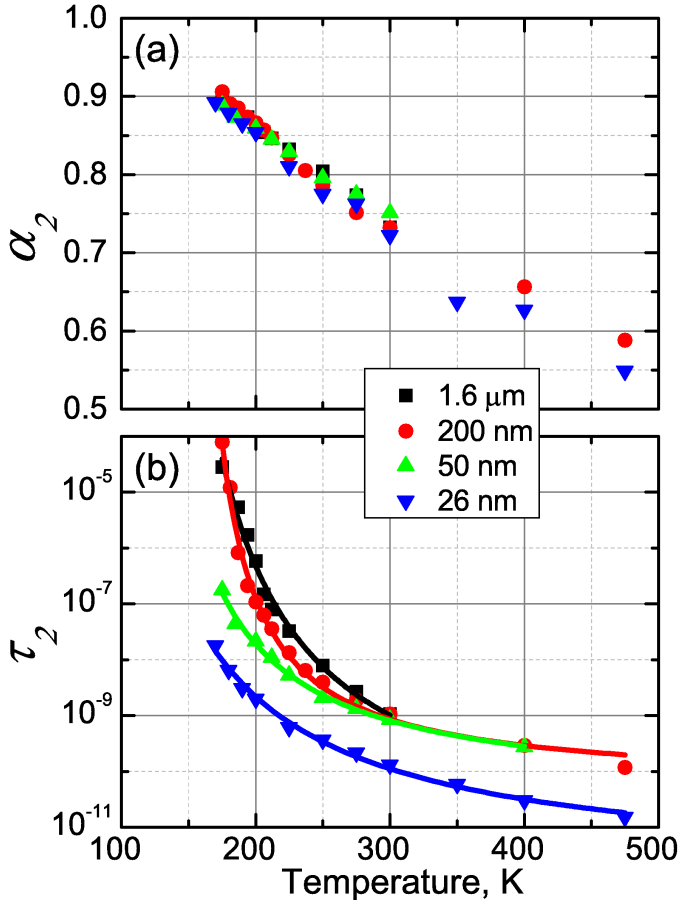

Figure 5.1.4. Temperature dependences of the distribution parameter (a) and the mean relaxation time (b) of the second process.

26 nm) the one with higher permittivity will have higher freezing temperature, lower activation energy and shorter attempt time. A possible explanation is to take grain boundary-dilution into account. It is very important to keep in mind that grain boundaries affect both static and dynamic properties, and the smaller the grains, the smaller relaxation time is to be expected. This is actually observed in our case (figure 5.1.4). However, this is absolutely not related to domain structure. The governing effect is grain boundary dilution and can be fully explained in the frame of effective medium theory [75], [94]. Shift of the relaxation time is even more difficult to predict in case of temperature-dependent properties of grains and grain boundaries. It is quite possible that the temperature dependence is altered by grain boundary dilution in such a way,

that the apparent freezing temperature is shifted, although in reality it is not. It is also possible that Vogel-Fulcher law is only valid in a limited temperature range. It would be possible to verify these assumptions if it was possible to obtain reliable fits very close to the reported freezing temperatures. Nonetheless, it is worth remarking that this relaxation is still present in the materials with the smallest grain size.

Freezing of domains, an unusual effect, has been previously observed in a well known ferroelectric KDP and its isomorphs [16], [74], [97], or even $BaTiO_3$ [13] (p. 512). One of the explanations of this process was pinning of domain walls at the tips (meeting points of domain walls and at crystal surfaces), the other - pinning to defects [98], and the contribution would be fully suppressed in crystals with high concentration of defects, when domain walls are fully pinned [16]. Study of the freezing process under variable AC amplitude is the best to show that the latter mechanism is most likely [99]. However, this type of freezing should be highly dependent on domain structure and type of the defects. Topology of domain structure could be dependent on grain size, and this would definitely influence the freezing temperature. It is unclear if density of the domain walls is important. The former is unlikely to be different among ceramics made from the same starting material using the same techniques. The latter is highly dependent on grain size [90]. The lack of clear size dependence of the freezing temperature and activation energy seem to suggest this process is not related to ferroelectric domains in case of BSPT. Furthermore, grains are expected to be monodomain at small grain sizes [90], and this has been experimentally confirmed [80]. Thus there should be no freezing in nanograined ceramics. However, it is still observed. This and the absence of a pronounced dependence of the freezing parameters on grain size makes domain freezing an unlikely process.

It is more likely, that this freezing is related to substitutional disorder in the material, as there are lots of experimental examples of link between the disorder in site occupancy and glass-like or relaxor-like processes in

ferroelectric state (e.g. [69], [72], [100]–[102] and many others). There is the same type of disorder in $BiScO_3$ – $PbTiO_3$ solid solutions. Furthermore, similar re-entrant relaxor-like process was already observed previously in 0.45BS-0.55PT [103] and $BaTiO_3$ – $BiScO_3$ solid solutions [104], [105]. It was found in [104] that upon addition of $BiScO_3$ non-contrast areas in piezoelectric force microscopy (PFM) images are formed, which still exhibit ferroelectric loops. This was explained by formation of polar nanoregions (PNR) which are smaller than PFM tip. These PNRs are likely to be stabilised by substitutional disorder in the ceramics and random electric fields, which arise from different charges of substituting ions (Ba^{+2}, Bi^{+3}, Sc^{+4}, Ti^{+5}). It is very likely that the very same PNRs are responsible for relaxor-like process in our case. An important difference from conventional relaxor materials would be that in our case PNRs (or other entities with short-ranged polar order) are embedded into a ferroelectric matrix, not into paraelectric one [106]. It is also possible, that domain walls influence the freezing of PNRs. The influence could be realised through strain [103]. This would make the observed anomaly to be a combined effect of PNRs and domain walls, with the PNRs being the governing entities. These persist below the crticial size, below which domains are not formed. This correlation could be one of the reasons for differences in freezing temperatures and activation energies, as domain structures are expected to be very different depending on grain size.

Very interesting is the third relaxational process, which is observed in coarse-grained ceramics only (figure 5.1.3, (a) and (e)). One of the important features of the process is the nearly temperature-independent relaxation frequency of 3 GHz. If this process is related to some polar entities only (i.e. PNRs or domain walls), then one would expect Arrhenius or Vogel-Fulcher type dependence. Similar high-frequency process with a temperature-independent relaxation time was previously observed in 0.36BS-0.64PT at lower frequencies [84]. On the other hand, these ceramics had 7.5 μm grains [85]. However, a more detailed analysis of SEM images in the latter paper

shows, that there are two types of grains – big (at least 10 μm) and small (around 6 μm). Furthermore, two overlapping processes can be distinguished in [84] – at around 0.3 GHz and 1 GHz. One can assume (as was done in [84]), that this process is related to acoustic emission at domain walls with constructive interference happening perpendicular to the walls. In that case fundamental mode depends on thickness of domains, and grain size dependence of relaxation time follows Kittel's law [107]. This was experimentally observed in BTO and PZT coarse-grained ceramics, and can be noticed in fine-grained BTO ceramics in [108]. However, values of relaxation frequencies in our case are following a linear dependence on grain size, which is more consistent with piezoelectric resonance inside the grain. A very similar effect was observed in KNN [109] – temperature independent relaxation frequency, which scales linearly with the grain size. Furthermore, product of relaxation frequency and grain size in case of BS-PT ceramics is $f \times D \approx 5$ km/s, which is very close to typical velocities of sound in solid bodies. The same product is close to 6 km/s in case of KNN, and this is the velocity of sound in KNN [110].

One of the crucial questions for this model is how we can excite the waves in a macroscopically unpoled sample. The reason hides in the fact, that there are domains inside the ferroelectric material. When external weak electric field is applied, then domain walls slightly move, emitting acoustic waves through coupling of polarization to strain (see i.e. [111]). The spectra of emitted waves would be quite broadband, as movement of the walls is actually jerky and associated with Barkhausen noise [112]. The noise emitted by different walls would then undergo interference. If there is a pattern of domain walls in the system, then some of the waves might become enhanced through constructive interference. A “herring-bone” (90°-domains inside 180°-domains) structure is formed in case of ceramics with large grains (above 10 μm and more in case of BTO [90] and PZT [113]). A more simple structure is observed in case of smaller grains – a stack of 90°-domains, each taking the

full cross-section of the grain [90], [108]. This means that, each of the domains can be approximated as a plate, which is resonating. If the plate is very thick, then it will be mechanically excited primarily in the thickness mode (i.e. BTO and PZT in [107]). However if diameter of the plate is big compared to its thickness, it will oscillate as a membrane. Wavelengths of fundamental oscillations of a membrane can be easily found (from, e.g. [114]) as $\lambda_{mn}=\pi d/\alpha_{mn}$, here α_{mn} is the n-th root of the m-th order Bessel function, d – diameter of the membrane. In case of fundamental oscillation, α_{01} = 2.405, and $\lambda_{01}=1.31d$. However, these membranes are connected into a single grain, and this means there is a very broad distribution of correlated oscillators. The mean radius of grain cross-section is smaller than the mean grain size by a factor of $\pi/2$ [115] (p. 295). If we take this into account, then $\lambda_{01}=0.83D$, here D is the mean diameter of the grains. This, basically, explains very close values of assumed wavelengths of the resonance frequencies and grain sizes. Moreover, high mechanical losses at microwave frequencies would increase the wavelength a little, and distribution of grain sizes would smear possible resonance-like dispersions into single Debye-like relaxation. Furthermore, mechanical losses are temperature-dependent, ant this can explain slight variation of relaxation frequency on temperature.

If we assume that inverse dependence of relaxation frequency on grain size is correct, then relaxation frequency should be around 20 GHz in case of 200 nm-sized grains, and that is still in our measurement range. However, it was only possible to measure the coarse-grained ceramics in 8-12 GHz band, and in case of all the others we have an empty window in 1 – 25 GHz range. Thus it becomes very difficult to discern the 3rd process with so few experimental data points, especially due to overlapping with a broader and quite stronger 2nd process. As a result, the 3rd process was fitted in case of coarse-grained ceramics only. However, this 3rd process might be the reason why there are small discrepancies between fit curves and experimental data in 26 – 40 GHz range (figure 5.1.3, (b-c) and (f-g)).

It is also possible that the grains are single domain in case of the nanograined ceramics [80]. In that case the wavelength of characteristic oscillation would be close to twice the diameter of the grain, i.e. it would be shifted to twice lower frequencies. However, the relaxation would still be undiscernable in the spectra due to lack of experimental data.

This particular process is the one which results in lower permittivity of coarse-grained ceramics at microwave frequencies (figure 5.1.2, (c) and (d)). In case of submicron and fine-grained ceramics the relaxation frequency of the process is close to or higher than 26 GHz, meaning that at all temperatures there is an extra contribution to permittivity compared to coarse-grained ceramics. This results in higher permittivity.

5.2. Modelling the size effects using effective medium approach

The data presented in figure 5.1.1 was given a deeper analysis from the perspective of grain size effect. In this work a generalised core-shell model (also known as generalised brick-wall model, see section 2.2.2, formula (10)) was applied. If shell thickness is assumed to be independent of grain size, then volume fraction of the shell can be calculated as follows:

$$x = 1 - \left(\frac{D - 2 \cdot d}{D} \right)^3 \qquad (23)$$

Here, D is diameter of the grain, d – thickness of the shell.

In our case there are 5 unknown parameters: real and imaginary parts of dielectric permittivity of the core and of the shell, and the thickness of the shell. Grain sizes are known from previous investigations [81]. On the other hand, 4 different grain sizes are available in our case, which leaves us with 8 experimental data points (both real and imaginary parts are taken into account). This allows to determine all the parameters without making any assumptions during optimisation procedure (data fitting). However, dielectric permittivity of

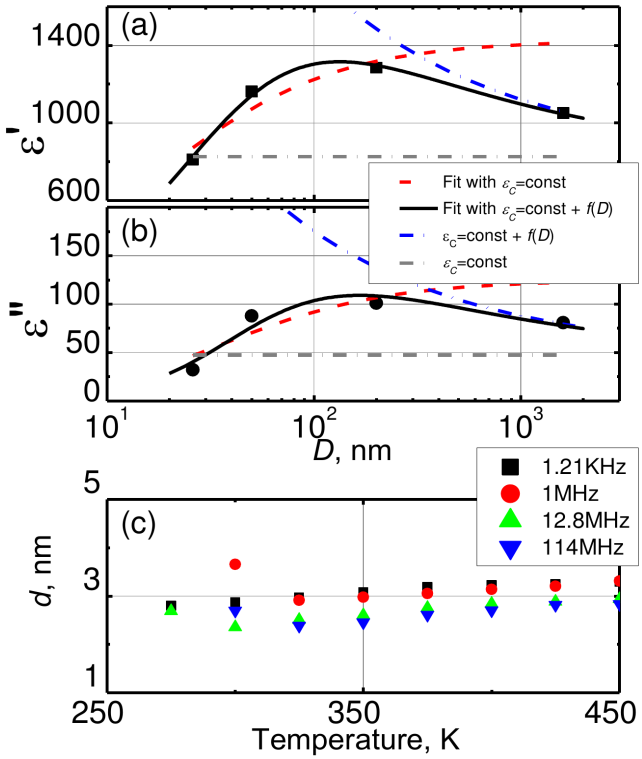

Figure 5.2.1. Grain size dependence of the real (a) and imaginary (b) parts of dielectric permittivity of ceramics; temperature dependence of the shell thickness at various frequencies (c).

coarse-grained ceramics is a little smaller than of submicron-grained ones. We decided to omit 1.6µm ceramics and apply the model to the remaining 3 sizes. A sample approximation is presented in figure 5.2.1, dashed line in (a) and (b). The fit is definitely not satisfactory. On the other hand, the reason for a non-monotonous size dependence of dielectric permittivity lies in the fact, that our material is a ferroelectric. This means that an additional contribution might come from domain walls. A similar maximum is observed in i.e. BTO [86]. Thus we decided to include the contribution to bulk material. It should be proportional to concentration of domain walls. It is known from literature, that domains are expected to be plate-like in ferroelectric ceramics, with domain size following Kittel's law [90], [91]. Thus we take into account size dependence of dielectric permittivity of the bulk material:

$$\varepsilon_c = \varepsilon_{c0} + \frac{A}{\sqrt{D}} \tag{24}$$

Here, ε_{c0} is grain size independent dielectric permittivity, and A is proportionality parameter for contribution of domain walls. A sample approximation is presented in figure 5.2.1, solid line in (a) and (b). As we can see, the approximation is much better, and it can include all the available experimental points. Furthermore, no restrictions were made during optimisation process to obtain the fit curve, as we have 8 experimental points, and there are 7 parameters to optimise (real and imaginary parts of ε_s, ε_{c0}, A and thickness of the shell d). One of the best ways to validate model is to check if temperature dependences of its parameters are sane. Figure 5.2.1 (c) contains temperature dependence of shell thickness at various frequencies. As we can see the thickness is nearly constant, as it should be in case of perfect core-shell structure, and is in the range of 2.5 – 3.5 nm. This means that the actual thickness of the inter-grain material is 5 – 7 nm.

One of the major issues with the model is the Kittel's law, o rather assumption that multidomain grains exist at all grain sizes. It is actually expected and was experimentally observed that grains must be single domain when grains are smaller than 100 nm [80], [90]. A possible explanation is that there might be some other entities contributing to dielectric permittivity, i.e. polar nanoregions, which are not the same as conventional ferroelectric domains. The material does act similarly to relaxor ferroelectrics at low temperatures, and this supports idea of polar nanoregions. It is also possible that there are structural nanotwins, which are expected to be present in a ferroelectric composition close to a morphotropic phase boundary [116], [117]. It is known that the twins can change their size under electric field (e.g. [118]), so they can give a contribution to dielectric permittivity.

Another interesting thing is that contribution of size-dependent process is quite large. Dash-dotted line in figure 5.2.1 (a) and (b) corresponds to formula (24). We can see that size-dependent contribution is around 20% to the real part

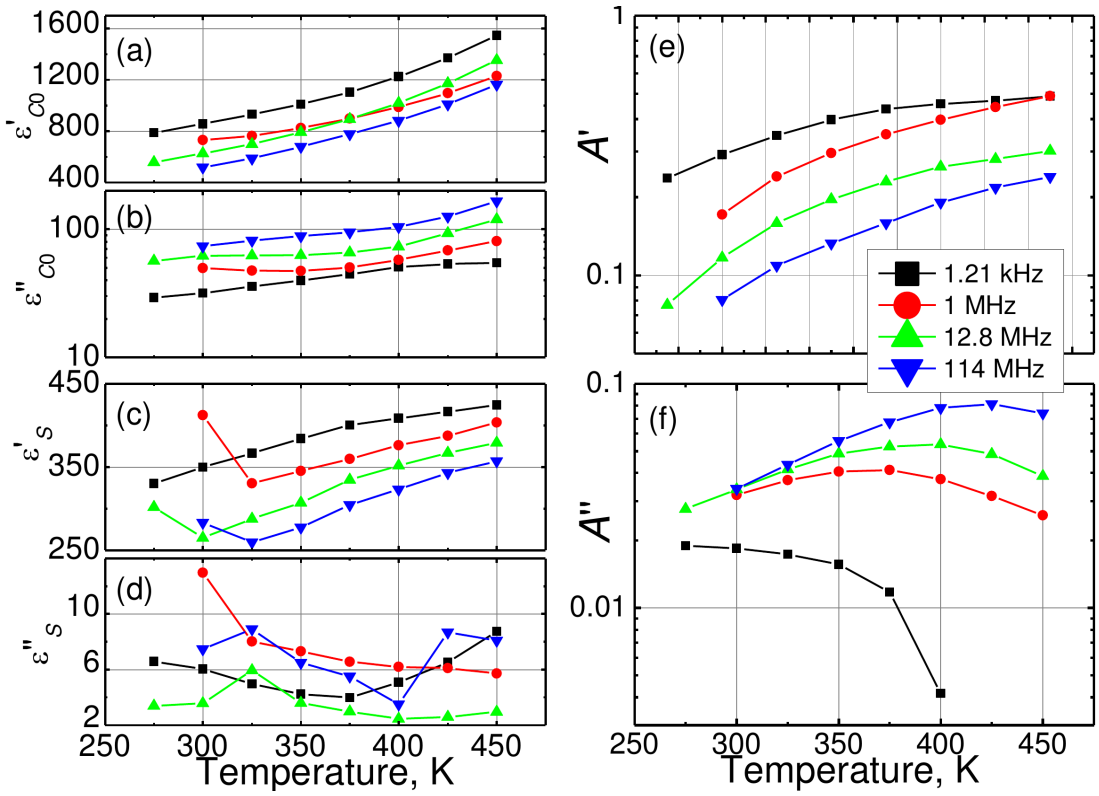

Figure 5.2.2. Temperature dependences of the real and imaginary parts of the grain size independent dielectric permittivity of the bulk material ((a) and (b)), of the shell material ((c) and (d)) and real and imaginary coefficients of contribution of grain size dependent contribution ((e) and (f)).

of permittivity value of grain core in case of coarse-grained ceramics, and reaches nearly 50% at submicron grains.

Figure 5.2.2 shows other fitting parameters, which allow to make further conclusions. Firstly, dielectric permittivity of the shell material is not as small as it is believed in case of BTO, which was assumed to be around 100 [86]. It is also interesting to note, that the material has quite small and frequency independent dielectric losses. However, the losses cannot be neglected, as the real part clearly shows frequency dependence. The dispersion is quite broad, and this means that the grain boundary material is quite disordered. The permittivity value, however, is quite similar to effective dielectric properties at 26 GHz of the ceramics (figure 5.1.1). This would also explain the lack of size dependence of the dielectric permittivity at high frequencies – dielectric

permittivity of the shell is numerically similar to the effective value, and this also means that it is close to dielectric permittivity of the bulk material. If the shell material has the same properties, it means that grain boundary dilution will not be observed. The same phenomenon happens at all frequencies at temperatures below 250 K. If there is no grain size effect, then no data can be extracted by application of EMA.

Secondly, size-independent part of dielectric permittivity of the core exhibits quite broad dipolar relaxation. The mean relaxation time is bound to correspond to frequencies higher than 100 MHz. It is very likely that the mean relaxation time is temperature independent. It is also important to note that this contribution might partially incorporate contribution of domain walls, which should be present in coarse-grained ceramics. This incorporation can be the source of fitting errors.

Thirdly, we can analyse temperature dependence of the size-dependent contribution (figure 5.2.2, (e) and (f)). Dielectric losses clearly show a frequency-dependent maximum. At low temperatures the losses become frequency-independent. This is quite similar to behaviour of ferroelectric relaxor materials. The same property is observable at lower temperatures in the ceramics themselves (figure 5.1.1). The shift of the temperature of the anomaly can be explained in the frame of EMA. The size-independent properties are temperature-dependent. All permittivities increase upon heating, while size-dependent contribution seems to saturate. This would lead to an apparent temperature shift of the anomaly related to the size-dependent process.

Another interesting detail is that the mean relaxation time is definitely temperature dependent in the latter case. We can see that at high temperatures losses are very close to 0 at frequencies below 1 MHz, and size-dependent permittivity is has the same value at 1 kHz and 1 MHz at 450 K. This means that relaxation time shortens upon heating. Frequency range of the relaxation must be finite at this temperature. Frequency-independent losses at low temperatures mean, on the other hand, infinitely broad dispersion region. This

means that the process becomes wider upon cooling. This is the same behaviour as in case of ferroelectric relaxors.

5.3. Summary

Broadband dielectric spectroscopy of $0.36BiScO_3$-$0.64PbTiO_3$ ceramics with decreasing average grain sizes from 1.6 μm down to 26 nm revealed several patterns. Firstly, the main contribution to dielectric permittivity in 150 – 500 K temperature range is inherently low-frequency, and it persists at the nanoscale. Its mean relaxation time follows Vogel-Fulcher law. The freezing parameters show no apparent dependence on grain size, which makes this contribution due to domain walls quite unlikely. It is proposed that there are polar nanoregions embedded into ferroelectric matrix and that there is correlation between PNRs and ferroelctric domains, with PNRs giving rise to Vogel-Fulcher behaviour of the low-frequency process. Furthermore, one more process is visible in GHz range, which has nearly temperature-independent relaxation time and is attributable to acoustic resonance of domains inside the grains. The latter explanation is based on the fact, that the characteristic relaxation frequency scales linearly with grain size, similarly to KNN.

The generalised core-shell effective medium model was applied to model properties of nonostructured ceramics of $0.36BiScO_3$-$0.64PbTiO_3$. We found, that thickness of the grain boundary is around 6 nm. Dielectric properties of the shell are temperature and frequency dependent with a broad dispersion region, meaning the medium is quite disordered. The crystallite material needs to be described by 2 contributions, one is size-independent, another depends on grain size with Kittel's law. The latter process gives important contribution to dielectric permittivity, and is the source of relaxor-like behaviour of the ceramics. The microscopic origin of the process is likely to be related to contribution of polar nanoregions or structural nanotwins rather than ferroelectric domains.

6. Experimental results: $BaSnO_3$ and Ba_2SnO_4

Some novel functionalities are known to be difficult to observe in perovskites, i.e. multiferroicity [119]. This means that search for novel non-perovskite materials is essential, too. On the other hand, perovskite materials can be viewed as the n=∞ of homologous series of oxides with stoichiometry $A_{n+1}B_nO_{3n+1}$, n=1, 2, …, ∞ (Ruddlesden – Popper series), so other structures in the series could be functional and suitable for applications.

Rare earth stannates (*A*=Ba, Ca, Sr, ...; *B*=Sn) are well known for different functionalities of their own. Perovskite $ASnO_3$ are important sensor materials to detect various gases [120]–[122]. They have also been studied for possible applications of the light-to-electrical and/or chemical energy conversion [123] and stable capacitors [124], [125].

$BaSnO_3$ is known to be a semiconducting perovskite with a wide bandgap of 3 – 3.4 eV [126], [127], with a cubic perovskite structure at room temperature with lattice constant of about 4.1 Å [128], [129]. It is known that conduction mechanism in perovskite materials is dominated by electrons, and their concentration is highly dependent on oxygen vacancies [130], [131]. There are a few studies of impedance properties of $BaSnO_3$, showing a single conductivity relaxation process, related to tin reduction upon formation of oxygen vacancies [132], [133]. This process should be dependent on specific surface area. However, to the best of our knowledge, impedance studies were only performed with bulk ceramics and never with nanostructured ones, although there are some reports on synthesis of fine powders [129], [134], [135].

Studies of Ba_2SnO_4 are even scarcer, as it is quite often considered to be a secondary phase to $BaSnO_3$. The material is known to have undistorted tetragonal symmetry in 12 – 295 K temperature range [136]. Sr_2SnO_4, on the other hand, is known to be orthorhombic at room temperature and undergoes a phase transition to orthorhombic structure with different tilting of oxygen

octahedra around 423 K and to tetragonal phase at around 573 K, which is again related to tilting of oxygen octahedra [137]. However, no similar studies have been performed with Ba_2SnO_4, so there still might be similar transitions happening without anyone knowing it. To the best of our knowledge, no impedance studies have been performed with this material, let alone nanostructured ceramics. That is why the aim of current contribution is to study nanostructured ceramics of $BaSnO_3$ and Ba_2SnO_4 by means of impedance spectroscopy and compare these materials.

6.1. Experimental

Nano-grained barium stannate powders were obtained via sol-gel synthesis route. The detailed procedure is presented elsewhere [138]. The resulting powders were grounded thoroughly and pressed into pellets with a diameter of 8 mm. The pellets were additionally heated at 800 °C and 1000 °C for 5 h in order to obtain dense ceramics of $BaSnO_3$ and Ba_2SnO_4, respectively.

Dielectric measurements were performed using precision LCR meter HP 4284A in 100 Hz – 1 MHz frequency range during cooling with 1K/min rate for both $BaSnO_3$ and Ba_2SnO_4 samples. In both cases sample was in form of pellet, $BaSnO_3$ and Ba_2SnO_4 were approximately 0.8 mm thick with silver paste used to produce contact area of around 8 mm^2. Temperature ranges were 300 K – 1000 K for both samples.

6.2. Experimental Results

As we can see from figures 6.2.1 and 6.2.2, dielectric spectra are dominated by conductivity in whole investigated temperature range, and no dielectric anomalies are observed. At low temperatures an increase in conductivity is observed on cooling in 320 K – 400 K temperature range. This is most likely related to humidity-induced conductivity in the sample, as

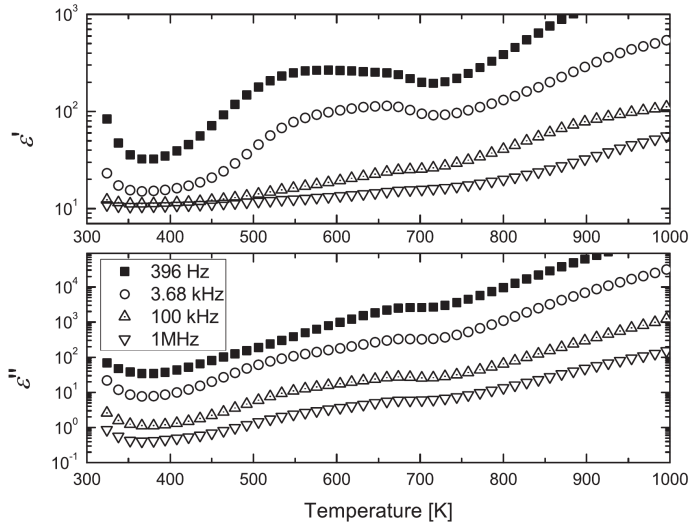

Figure 6.2.1. Temperature dependence of the real and imaginary parts of complex dielectric permittivity of $BaSnO_3$.

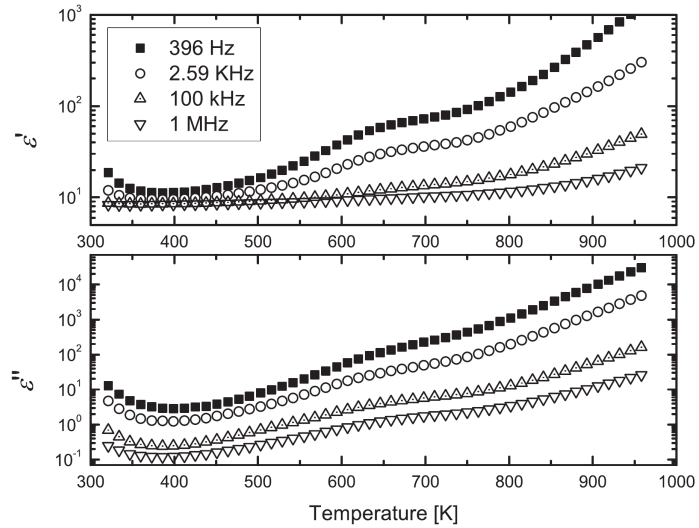

Figure 6.2.2. Temperature dependence of the real and imaginary parts of complex dielectric permittivity of Ba_2SnO_4.

material is not hydrophobic and is highly porous due to nanostructured nature. At high temperatures humidity of air is relatively low, and dielectric losses are dominated by material's conductivity. At temperatures below 400 K humidity influences measured impedance a lot. This fact is known for $BaSnO_3$, as it is a good humidity sensor material [121]. Apparently, Ba_2SnO_4 is a good sensor material, too.

At low frequencies dielectric spectra are dominated by conduction mechanisms. However, at high frequencies very low complex dielectric permittivity ($\varepsilon^* = \varepsilon' - j\varepsilon''$) was observed. This is due to both relatively low dielectric permittivity of the material and relatively low density of the ceramic. Dielectric permittivity spectra were not informative for further analysis, so specific impedance was calculated from these results.

Figures 6.2.3 and 6.2.4 show frequency dependencies of specific impedance of both ceramics. The important difference between the materials is that there are two processes observable in $BaSnO_3$ at temperature below 700 K, with the high frequency process disappearing from the spectra due to frequency limitations of the experiment. We argue that the low-frequency process is due to inter-grain charge relaxation, while high frequency process is due to relaxation inside grains of the ceramics. On the other hand, there is only one process observed in Ba_2SnO_4 besides very high temperatures (> 800 K), when at low frequencies a second process appears. The latter one is most likely due to contact effects, and the former – inter-grain relaxation.

Solid lines in figures 6.2.3 and 6.2.4 represent data fits. Formula (25) was used in cases where only one process is observed. This formula corresponds to parallel RC circuit with constant phase element (CPE) instead of normal capacitance. ρ_0 corresponds to specific resistivity of the process (in relation to the total volume of the sample, not just inter-grain volume for example), τ is relaxation time of the process, and α is related to characteristic exponent of the CPE, or, alternatively, it could be related to a distribution of RC circuits with different relaxation times. α=0 corresponds to a single parallel RC circuit with conventional capacitance. ω is angular frequency.

$$\rho^* = \frac{\rho_0}{1+(i\omega\tau)^{(1-\alpha_0)}} \qquad (25)$$

In cases where two processes where observed, formula (26) was used. It corresponds to serial connection of two parallel RC circuits.

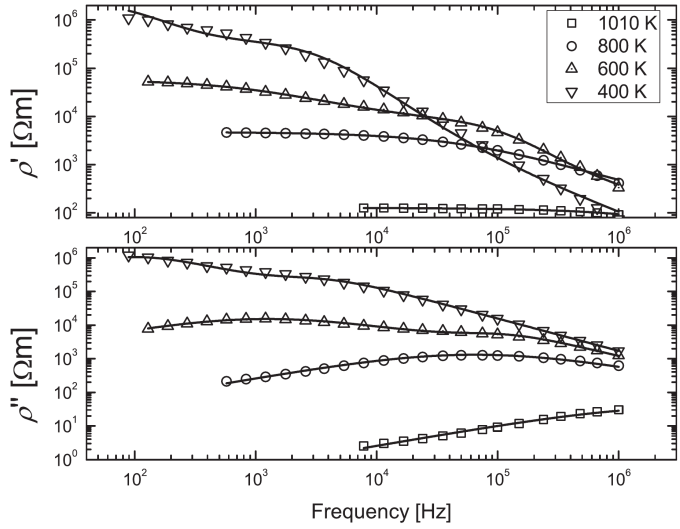

Figure 6.2.3. Frequency dependences of the real and imaginary parts of specific impedance of $BaSnO_3$.

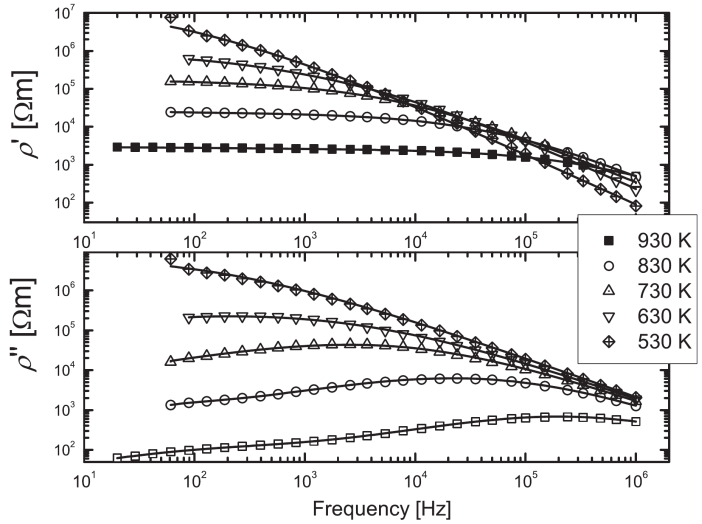

Figure 6.2.4. Frequency dependences of the real and imaginary parts of specific impedance of Ba_2SnO_4.

$$\rho^* = \frac{\rho_1}{1+\left(i\omega\tau_1\right)^{(1-\alpha_1)}} + \frac{\rho_2}{1+\left(i\omega\tau_2\right)^{(1-\alpha_2)}} \tag{26}$$

$$\rho = \rho_0 e^{E_a/kT} \tag{27}$$

Frequencies of maxima in imaginary part of impedances correspond to reciprocal relaxation times. We can see from frequency dependencies, that the higher the temperature, the shorter the time. This is likely related to decrease of

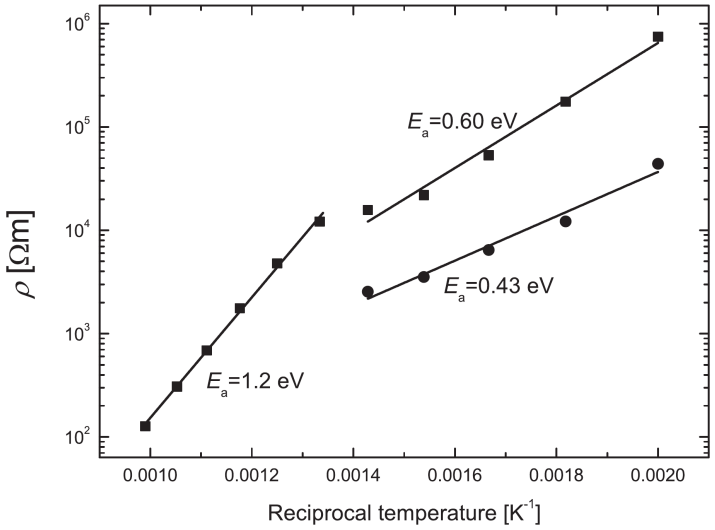

Figure 6.2.5. Reciprocal temperature dependence of the DC specific resistivity of $BaSnO_3$.

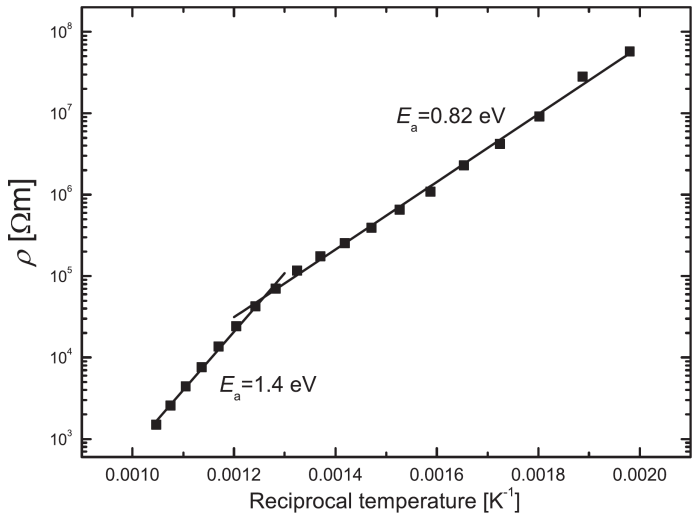

Figure 6.2.6. Reciprocal temperature dependence of the DC specific resistivity of Ba_2SnO_4.

resistivity at higher temperatures. The latter fact is especially obvious from reciprocal temperature dependencies of specific resistivity, which are plotted in fig. 6.2.5 and fig. 6.2.6. These graphs show Arrhenius-type behavior, that is why experimental data was fitted with equation (27) (solid lines in the figures). It was found that in case of $BaSnO_3$ at temperatures above 700 K activation energy of inter-grain process is 1.2 eV, while below it is equal to 0.60 eV. Bulk conductivity in the same temperature range has activation energy of 0.43 eV.

Inter-grain conductivity of Ba_2SnO_4 has activation energy of 1.4 eV at temperatures above 800 K and 0.82 eV below.

$BaSnO_3$ has smaller specific resistivity and lower activation energies when compared to Ba_2SnO_4. However, the values of activation energies obtained here are higher than values obtained elsewhere (e.g. at lower temperatures activation energy is 0.3 eV in [133] and 0.16 eV in [126]). One thing in common for both materials is that there is a change of activation energy. Similar effects where observed in [126], [132]. This change must be related to change in mechanism of electric conductivity. There actually are two different probable explanations.

The first explanation is purely electronic mechanisms. The ceramic samples are white. This means they are quite stoichiometric [139]. It is possible that there are some contaminants with quite low concentration and at low temperatures conductivity is dominated by electrons (or possibly holes) derived from shallow dopants. At high temperatures natural conductivity by electrons near Fermi level starts to dominate (intrinsic conductivity). This mechanism cannot be ruled out, as in case of $BaSnO_3$ bandgap is around 3 eV, and activation energy is 1.2 eV, which does not differ much from $0.5E_g$. Bandgap of barium orthostannate is not known, but it should be quite similar.

Another possible mechanism is related to oxygen vacancies. At low temperatures conductivity is dominated by electrons, which are freed upon oxygen escape, that is when oxygen vacancies form, but they are immobile. At higher temperatures oxygen vacancies gain mobility and start to dominate charge transfer. It is known for other perovskite materials that activation energy of mobile oxygen vacancies is around 0.6 – 1.5 eV [140], [141], while electronic conductivity related to immobile oxygen vacancies is reported to have activation energy in 0.3 – 1 eV range depending on material and on charge of the vacancy (single ionised or double ionised state) [141]. In case of orthostannates it is likely to be a very similar case. Based on these values this mechanism is quite plausible, too. Of course, in reality it could be a

combination of the processes, but it is very difficult to determine the actual mechanism from these studies alone.

6.3. Summary

Dielectric and impedance spectroscopy studies of barium stannate ($BaSnO_3$) and barium orthostannate (Ba_2SnO_4) were performed. The experimental results showed that both materials do not exhibit any dielectric anomalies in 300 – 1000 K temperature range. Both materials are sensitive to humidity of air. $BaSnO_3$ showed two charge transfer processes in 20 Hz – 1 MHz frequency and 300 – 700 K temperature ranges. In both materials DC conductivity is thermally activated and follows Arrhenius equation. Both materials have a change of activation energies – from 0.60 eV to 1.2 eV at 700 K ($BaSnO_3$) and from 0.82 eV to 1.4 eV at 800 K (Ba_2SnO_4). This process is most likely happening in inter-grain region. Bulk conductivity is observed only in $BaSnO_3$ below 700 K with activation energy of 0.43 eV. At low temperatures charge transfer is dominated by electronic conductivity, originating from dopants or immobile oxygen vacancies. At high temperatures main conductivity process could be either intrinsic electronic conductivity or ionic conductivity by mobile oxygen vacancies.

7. Conclusions

1. In case of relaxors, bulk properties are mostly defined by polar nanoregions. Grain size heavily influences their contribution. Grain boundaries limit growth and interaction of the nanoregions. However, some interactions between adjacent grains are still present in ceramics.
2. Spontaneous phase transition in PSN is not driven by polar nanoregions alone, although they modify the ground state.
3. A contribution of some polar and nanoscopic entities (likely similar or the same as polar nanoregions in relaxors) is present in 0.36BS-0.64PT ceramics, which gives rise to Vogel-Fulcher behaviour in the material, unlike the expected Arrhenius one. It is likely that similar entities can be observed in other ferroelectrics.
4. Concentration of the nanoscopic polar entities in 0.36BS-0.64PT ceramics depends on grain size in accordance with Kittel's law.
5. Effective medium approximation can explain evolution of dielectric properties of ferroelectrics and relaxors only if dependence of bulk properties on grain size is known.
6. Both $BaSnO_3$ and $BaSn_2O_4$ do not exhibit any dielectric anomalies in 300 – 1000 K temperature range and are sensitive to humidity of air. Dielectric spectra are dominated by conductivity, which, at high temperatures, arises from intrinsic electronic conductivity or ionic conductivity by mobile oxygen vacancies.

8. References

[1] K. S. Cole and R. H. Cole, “Dispersion and Absorption in Dielectrics I. Alternating Current Characteristics,” *J. Chem. Phys.*, vol. 9, no. 4, pp. 341–351, Apr. 1941.

[2] S. Havriliak and S. Negami, “A complex plane representation of dielectric and mechanical relaxation processes in some polymers,” *Polymer*, vol. 8, pp. 161–210, 1967.

[3] R. Zorn, “Logarithmic moments of relaxation time distributions,” *J Chem Phys*, vol. 116, no. 8, p. 3204, 2002.

[4] I. Rychetský and J. Petzelt, “Dielectric properties of ferroelectric powders and microcomposites,” *Ferroelectrics*, vol. 236, no. 1, pp. 223–234, 2000.

[5] I. Rychetský, O. Hudák, and J. Petzelt, “Dielectric properties of microcomposite ferroelectrics,” *Phase Transit.*, vol. 67, no. 4, pp. 725–739, 1999.

[6] D. J. Bergman, “The dielectric constant of a composite material—A problem in classical physics,” *Phys. Rep.*, vol. 43, no. 9, pp. 377–407, Jul. 1978.

[7] N. J. Kidner, N. H. Perry, T. O. Mason, and E. J. Garboczi, “The Brick Layer Model Revisited: Introducing the Nano-Grain Composite Model,” *J. Am. Ceram. Soc.*, vol. 91, no. 6, pp. 1733–1746, Jun. 2008.

[8] Z. Hashin and S. Shtrikman, “A Variational Approach to the Theory of the Effective Magnetic Permeability of Multiphase Materials,” *J. Appl. Phys.*, vol. 33, no. 10, pp. 3125–3131, Oct. 1962.

[9] I. RYCHETSKY and J. PETZELT, “Dielectric Spectra of Grainy High-Permittivity Materials,” *Ferroelectrics*, vol. 303, no. 1, pp. 137–140, 2004.

[10] J. Valasek, “Piezo-Electric and Allied Phenomena in Rochelle Salt,” *Phys. Rev.*, vol. 17, no. 4, pp. 475–481, Apr. 1921.

[11] C. Kittel, *Introduction to Solid State Physics*. 2004.

[12] C. Kittel, “Theory of the Structure of Ferromagnetic Domains in Films and Small Particles,” *Phys Rev*, vol. 70, no. 11–12, pp. 965–971, Dec. 1946.

[13] A. K. Tagantsev, L. E. Cross, and J. Fousek, *Domains in Ferroic Crystals and Thin Films*. New York, NY: Springer New York, 2010.

[14] P. Marton, I. Rychetsky, and J. Hlinka, “Domain walls of ferroelectric $BaTiO_3$ within the Ginzburg-Landau-Devonshire phenomenological model,” *Phys. Rev. B*, vol. 81, no. 14, p. 144125, Apr. 2010.

[15] B. L. Cheng, M. Gabbay, M. Maglione, Y. Jorand, and G. Fantozzi, “Domain Walls Motions in Barium Titanate Ceramics,” *J. Phys. IV*, vol. 06, no. C8, pp. C8–647–C8–650, Dec. 1996.

[16] E. Nakamura, “Anomalous dielectric behavior of KH_2PO_4 type crystals in the ferroelectric phase,” *Ferroelectrics*, vol. 135, no. 1, pp. 237–247,

1992.
[17] Y. L. Wang, A. K. Tagantsev, D. Damjanovic, and N. Setter, “Giant domain wall contribution to the dielectric susceptibility in BaTiO3 single crystals,” *Appl. Phys. Lett.*, vol. 91, no. 6, p. 062905, Aug. 2007.
[18] Y. L. Wang, Z. B. He, D. Damjanovic, A. K. Tagantsev, G. C. Deng, and N. Setter, “Unusual dielectric behavior and domain structure in rhombohedral phase of $BaTiO_3$ single crystals,” *J. Appl. Phys.*, vol. 110, no. 1, p. 014101, Jul. 2011.
[19] S.-E. Park and T. R. Shrout, “Ultrahigh strain and piezoelectric behavior in relaxor based ferroelectric single crystals,” *J. Appl. Phys.*, vol. 82, no. 4, pp. 1804–1811, Aug. 1997.
[20] G. Burns and F. H. Dacol, “Glassy polarization behavior in ferroelectric compounds Pb(Mg13Nb23)O3 and Pb(Zn13Nb23)O3,” *Solid State Commun.*, vol. 48, no. 10, pp. 853–856, Dec. 1983.
[21] R. A. Cowley, S. N. Gvasaliya, S. G. Lushnikov, B. Roessli, and G. M. Rotaru, “Relaxing with relaxors: a review of relaxor ferroelectrics,” *Adv. Phys.*, vol. 60, no. 2, pp. 229–327, 2011.
[22] J. Hlinka, J. Petzelt, S. Kamba, D. Noujni, and T. Ostapchuk, “Infrared dielectric response of relaxor ferroelectrics,” *Phase Transit.*, vol. 79, no. 1–2, pp. 41–78, 2006.
[23] D. Fu, H. Taniguchi, M. Itoh, S. Koshihara, N. Yamamoto, and S. Mori, “Relaxor Pb(Mg1/3Nb2/3)O3: A Ferroelectric with Multiple Inhomogeneities,” *Phys. Rev. Lett.*, vol. 103, no. 20, p. 207601, Nov. 2009.
[24] N. Novak, R. Pirc, M. Wencka, and Z. Kutnjak, “High-Resolution Calorimetric Study of Pb(Mg1/3Nb2/3)O3 Single Crystal,” *Phys. Rev. Lett.*, vol. 109, no. 3, p. 037601, Jul. 2012.
[25] J. Macutkevic, S. Kamba, J. Banys, A. Brilingas, A. Pashkin, J. Petzelt, K. Bormanis, and A. Sternberg, “Infrared and broadband dielectric spectroscopy of PZN-PMN-PSN relaxor ferroelectrics: Origin of two-component relaxation,” *Phys. Rev. B*, vol. 74, no. 10, p. 104106, Sep. 2006.
[26] D. Viehland, S. J. Jang, L. E. Cross, and M. Wuttig, “Freezing of the polarization fluctuations in lead magnesium niobate relaxors,” *J. Appl. Phys.*, vol. 68, no. 6, pp. 2916–2921, Sep. 1990.
[27] F. Chu, N. Setter, and A. K. Tagantsev, “The spontaneous relaxor-ferroelectric transition of $Pb(Sc_{0.5}Ta_{0.5})O_3$,” *J. Appl. Phys.*, vol. 74, no. 8, pp. 5129–5134, Oct. 1993.
[28] X. Dai, Z. Xu, and D. Viehland, “The spontaneous relaxor to normal ferroelectric transformation in La-modified lead zirconate titanate,” *Philos. Mag. Part B*, vol. 70, no. 1, pp. 33–48, 1994.
[29] A. Krumins, T. Shiosaki, and S. Koizumi, “Spontaneous Trasition between Relaxor and Ferroelectric States in Lanthanum-Modified Lead Zirconate Titanate (6–7)/65/35,” *Jpn. J. Appl. Phys.*, vol. 33, no. Part 1,

No. 9A, pp. 4940–4945, 1994.
[30] P. Sciau, G. Calvarin, and J. Ravez, “X-ray diffraction study of BaTi0.65Zr0.35O3 and Ba0.92Ca0.08Ti0.75Zr0.25O3 compositions: influence of electric field,” *Solid State Commun.*, vol. 113, no. 2, pp. 77–82, Nov. 1999.
[31] A. Simon, J. Ravez, and M. Maglione, “The crossover from a ferroelectric to a relaxor state in lead-free solid solutions,” *J. Phys. Condens. Matter*, vol. 16, no. 6, p. 963, Feb. 2004.
[32] N. Yasuda, H. Ohwa, and S. Asano, “Dielectric Properties and Phase Transitions of $\bf Ba(Ti_1-\ninmbixSn_\ninmbix)O_3$ Solid Solution,” *Jpn. J. Appl. Phys.*, vol. 35, no. Part 1, No. 9B, pp. 5099–5103, 1996.
[33] J. Macutkevic, J. Banys, R. Grigalaitis, and Y. Vysochanskii, “Asymmetric phase diagram of mixed CuInP2(SxSe1−x)6 crystals,” *Phys. Rev. B*, vol. 78, no. 6, Aug. 2008.
[34] M. E. Manley, J. W. Lynn, D. L. Abernathy, E. D. Specht, O. Delaire, A. R. Bishop, R. Sahul, and J. D. Budai, “Phonon localization drives polar nanoregions in a relaxor ferroelectric,” *Nat. Commun.*, vol. 5, Apr. 2014.
[35] A. R. Bishop, A. Bussmann-Holder, S. Kamba, and M. Maglione, “Common characteristics of displacive and relaxor ferroelectrics,” *Phys. Rev. B*, vol. 81, no. 6, p. 064106, Feb. 2010.
[36] J. Macutkevic, J. Banys, A. Bussmann-Holder, and A. R. Bishop, “Origin of polar nanoregions in relaxor ferroelectrics: Nonlinearity, discrete breather formation, and charge transfer,” *Phys. Rev. B*, vol. 83, no. 18, p. 184301, May 2011.
[37] S. J. Patwe, S. N. Achary, J. Manjanna, A. K. Tyagi, S. K. Deshpande, S. K. Mishra, P. S. R. Krishna, and A. B. Shinde, “Observation of a new cryogenic temperature dielectric relaxation in multiferroic Bi7Fe3Ti3O21,” *Appl. Phys. Lett.*, vol. 103, no. 12, p. 122901, Sep. 2013.
[38] J. Macutkevic, J. Banys, and R. Grigalaitis, “Comment on ‘Revisit of the Vogel–Fulcher freezing in lead magnesium niobate relaxors’ [Appl. Phys. Lett.97, 132905 (2010)],” *Appl. Phys. Lett.*, vol. 98, no. 1, p. 016101, Jan. 2011.
[39] R. Pirc and R. Blinc, “Vogel-Fulcher freezing in relaxor ferroelectrics,” *Phys. Rev. B*, vol. 76, no. 2, p. 020101, Jul. 2007.
[40] S. Prosandeev, D. Wang, A. R. Akbarzadeh, B. Dkhil, and L. Bellaiche, “Field-Induced Percolation of Polar Nanoregions in Relaxor Ferroelectrics,” *Phys. Rev. Lett.*, vol. 110, no. 20, p. 207601, May 2013.
[41] A. Koreeda, H. Taniguchi, S. Saikan, and M. Itoh, “Fractal Dynamics in a Single Crystal of a Relaxor Ferroelectric,” *Phys. Rev. Lett.*, vol. 109, no. 19, p. 197601, Nov. 2012.
[42] M. B. Smith, K. Page, T. Siegrist, P. L. Redmond, E. C. Walter, R. Seshadri, L. E. Brus, and M. L. Steigerwald, “Crystal Structure and the Paraelectric-to-Ferroelectric Phase Transition of Nanoscale BaTiO3,” *J.*

Am. Chem. Soc., vol. 130, no. 22, pp. 6955–6963, Jun. 2008.
[43] C. A. Randall, N. Kim, J.-P. Kucera, W. Cao, and T. R. Shrout, “Intrinsic and Extrinsic Size Effects in Fine-Grained Morphotropic-Phase-Boundary Lead Zirconate Titanate Ceramics,” *J. Am. Ceram. Soc.*, vol. 81, no. 3, pp. 677–688, Mar. 1998.
[44] S. Lin, T. Lü, C. Jin, and X. Wang, “Size effect on the dielectric properties of $BaTiO_3$ nanoceramics in a modified Ginsburg-Landau-Devonshire thermodynamic theory,” *Phys. Rev. B*, vol. 74, no. 13, p. 134115, Oct. 2006.
[45] A. Y. Emelyanov, N. A. Pertsev, S. Hoffmann-Eifert, U. Böttger, and R. Waser, “Grain-Boundary Effect on the Curie-Weiss Law of Ferroelectric Ceramics and Polycrystalline Thin Films: Calculation by the Method of Effective Medium,” *J. Electroceramics*, vol. 9, no. 1, pp. 5–16, Oct. 2002.
[46] M. M. Saad, P. Baxter, R. M. Bowman, J. M. Gregg, F. D. Morrison, and J. F. Scott, “Intrinsic dielectric response in ferroelectric nano-capacitors,” *J. Phys. Condens. Matter*, vol. 16, no. 41, p. L451, Oct. 2004.
[47] V. Buscaglia, M. T. Buscaglia, M. Viviani, L. Mitoseriu, P. Nanni, V. Trefiletti, P. Piaggio, I. Gregora, T. Ostapchuk, J. Pokorný, and J. Petzelt, “Grain size and grain boundary-related effects on the properties of nanocrystalline barium titanate ceramics,” *J. Eur. Ceram. Soc.*, vol. 26, no. 14, pp. 2889–2898, 2006.
[48] J. Carreaud, P. Gemeiner, J. M. Kiat, B. Dkhil, C. Bogicevic, T. Rojac, and B. Malic, “Size-driven relaxation and polar states in PbMg1⁄3Nb2⁄3O3-based system,” *Phys. Rev. B*, vol. 72, no. 17, p. 174115, Nov. 2005.
[49] R. Jiménez, H. Amorín, J. Ricote, J. Carreaud, J. M. Kiat, B. Dkhil, J. Holc, M. Kosec, and M. Algueró, “Effect of grain size on the transition between ferroelectric and relaxor states in 0.8Pb(Mg1/3Nb2/3)O3-0.2PbTiO3 ceramics,” *Phys. Rev. B*, vol. 78, no. 9, p. 094103, Sep. 2008.
[50] J. Carreaud, J. M. Kiat, B. Dkhil, M. Algueró, J. Ricote, R. Jiménez, J. Holc, and M. Kosec, “Monoclinic morphotropic phase and grain size-induced polarization rotation in Pb(Mg1⁄3Nb2⁄3)O3–PbTiO3,” *Appl. Phys. Lett.*, vol. 89, no. 25, p. 252906, Dec. 2006.
[51] M. Algueró, J. Ricote, R. Jiménez, P. Ramos, J. Carreaud, B. Dkhil, J. M. Kiat, J. Holc, and M. Kosec, “Size effect in morphotropic phase boundary Pb(Mg1⁄3Nb2⁄3)O3–PbTiO3,” *Appl. Phys. Lett.*, vol. 91, no. 11, p. 112905, Sep. 2007.
[52] J. Carreaud, C. Bogicevic, B. Dkhil, and J. M. Kiat, “Dielectric evidences of core-shell-like effects in nanosized relaxor PbMg1⁄3Nb2⁄3O3,” *Appl. Phys. Lett.*, vol. 92, no. 24, p. 242902, Jun. 2008.
[53] V. Bovtun, S. Kamba, S. Veljko, D. Nuzhnyy, J. Kroupa, M. Savinov, P. Vaněk, J. Petzelt, J. Holc, M. Kosec, H. Amorín, and M. Alguero,

"Broadband dielectric spectroscopy of phonons and polar nanoclusters in $PbMg_{1/3}Nb_{2/3}O_3$-35%$PbTiO_3$ ceramics: Grain size effects," *Phys. Rev. B*, vol. 79, no. 10, p. 104111, Mar. 2009.

[54] P. Papet, J. P. Dougherty, and T. R. Shrout, "Particle and grain size effects on the dielectric behavior of the relaxor ferroelectric Pb(Mg1/3Nb2/3)O3," *J. Mater. Res.*, vol. 5, no. 12, pp. 2902–2909, 1990.

[55] J. Grigas, *Microwave Dielectric Spectroscopy of Ferroelectrics and Related Materials*. 1996.

[56] A. A. BOKOV and Z.-G. YE, "DIELECTRIC RELAXATION IN RELAXOR FERROELECTRICS," *J. Adv. Dielectr.*, vol. 02, no. 02, p. 1241010, 2012.

[57] W. Kleemann, "The relaxor enigma — charge disorder and random fields in ferroelectrics," in *Frontiers of Ferroelectricity*, Springer US, 2007, pp. 129–136.

[58] J. BANYS, R. GRIGALAITIS, M. IVANOV, J. CARREAUD, and J. M. KIAT, "Dielectric Behaviour of a Nanograin Pmn Powders," *Integr. Ferroelectr.*, vol. 99, no. 1, pp. 132–139, 2008.

[59] R. Grigalaitis, J. Banys, A. Kania, and A. Slodczyk, "Distribution of relaxation times in PMN single crystal," *J. Phys. IV Proc.*, vol. 128, pp. 127–131, Sep. 2005.

[60] R. Grigalaitis, J. Banys, A. Sternberg, K. Bormanis, and V. Zauls, "Dynamics of Polar Clusters in PMN Ceramics: Comparison with PMN Single Crystal," *Ferroelectrics*, vol. 340, no. 1, pp. 147–153, 2006.

[61] R. Grigalaitis, M. Ivanov, J. Macutkevic, J. Banys, J. Carreaud, J. M. Kiat, V. V. Laguta, and B. Zalar, "Size effects in a relaxor: further insights into PMN," *J. Phys. Condens. Matter*, vol. 26, no. 27, p. 272201, Jul. 2014.

[62] Z. Zhao, V. Buscaglia, M. Viviani, M. T. Buscaglia, L. Mitoseriu, A. Testino, M. Nygren, M. Johnsson, and P. Nanni, "Grain-size effects on the ferroelectric behavior of dense nanocrystalline BaTiO3 ceramics," *Phys. Rev. B*, vol. 70, no. 2, p. 024107, Jul. 2004.

[63] R. Grigalaitis, J. Banys, S. Lapinskas, E. Erdem, R. Boettcher, H. J. Glaesel, and E. Hartmann, "Dielectric Investigations and Theoretical Calculations of Size Effect in Lead Titanate Nanocrystals," *Mater. Sci. Forum*, vol. 514–516, pp. 235–239, 2006.

[64] N. de Mathan, E. Husson, G. Calvarn, J. R. Gavarri, A. W. Hewat, and A. Morell, "A structural model for the relaxor PbMg1/3Nb2/3O3 at 5 K," *J. Phys. Condens. Matter*, vol. 3, no. 42, p. 8159, Oct. 1991.

[65] G. Xu, G. Shirane, J. R. D. Copley, and P. M. Gehring, "Neutron elastic diffuse scattering study of Pb(Mg1/3Nb2/3)O3," *Phys. Rev. B*, vol. 69, no. 6, p. 064112, Feb. 2004.

[66] J. Rault, "Origin of the Vogel–Fulcher–Tammann law in glass-forming materials: the α–β bifurcation," *J. Non-Cryst. Solids*, vol. 271, no. 3, pp.

177–217, Jul. 2000.
[67] E. V. Colla, E. Y. Koroleva, N. M. Okuneva, and S. B. Vakhrushev, “Low-frequency dielectric response of PbMg1/3Nb2/3O3,” *J. Phys. Condens. Matter*, vol. 4, no. 13, p. 3671, Mar. 1992.
[68] F. Chu, I. M. Reaney, and N. Setter, “Spontaneous (zero-field) relaxor–to–ferroelectric-phase transition in disordered $Pb(Sc_{1/2}Nb_{1/2})O_3$,” *J. Appl. Phys.*, vol. 77, no. 4, pp. 1671–1676, Feb. 1995.
[69] S. Svirskas, M. Ivanov, S. Bagdzevicius, J. Macutkevic, A. Brilingas, J. Banys, J. Dec, S. Miga, M. Dunce, E. Birks, M. Antonova, and A. Sternberg, “Dielectric properties of $0.4Na_{0.5}Bi_{0.5}TiO_3$–$(0.6\text{-}x)SrTiO_3$–$xPbTiO_3$ solid solutions,” *Acta Mater.*, vol. 64, pp. 123–132, Feb. 2014.
[70] J. M. Kiat, C. Bogicevic, F. Karolak, G. Dezanneau, N. Guiblin, W. Ren, L. Bellaiche, and R. Haumont, “Low-symmetry phases and loss of relaxation in nanosized lead scandium niobate,” *Phys Rev B*, vol. 81, no. 14, p. 144122, Apr. 2010.
[71] M. Ivanov, J. Banys, C. Bogicevic, and J.-M. Kiat, “Size Effects on Dielectric Properties of Nanograin PSN Ceramics,” *Ferroelectrics*, vol. 429, no. 1, pp. 43–47, 2012.
[72] Z. Trybula, V. H. Schmidt, and J. E. Drumheller, “Coexistence of proton-glass and ferroelectric order in $Rb_{1-x}(NH_4)_xH_2AsO_4$,” *Phys. Rev. B*, vol. 43, no. 1, pp. 1287–1289, Jan. 1991.
[73] B. L. Cheng, M. Gabbay, and G. Fantozzi, “Anelastic relaxation associated with the motion of domain walls in barium titanate ceramics,” *J. Mater. Sci.*, vol. 31, no. 15, pp. 4141–4147, Jan. 1996.
[74] P. Kubinec, M. Fally, A. Fuith, H. Kabelka, and C. Filipic, “A dielectric study of the domain freezing in KH_2AsO_4,” *J. Phys. Condens. Matter*, vol. 7, no. 10, p. 2205, Mar. 1995.
[75] J. Petzelt, I. Rychetsky, and D. Nuzhnyy, “Dynamic Ferroelectric–Like Softening Due to the Conduction in Disordered and Inhomogeneous Systems: Giant Permittivity Phenomena,” *Ferroelectrics*, vol. 426, no. 1, pp. 171–193, 2012.
[76] G. H. Haertling, “Ferroelectric Ceramics: History and Technology,” *J. Am. Ceram. Soc.*, vol. 82, no. 4, pp. 797–818, Apr. 1999.
[77] I. Coondoo, N. Panwar, and A. Kholkin, “Lead-free piezoelectrics: Current status and perspectives,” *J. Adv. Dielectr.*, vol. 03, no. 02, p. 1330002, Apr. 2013.
[78] T. Takenaka and H. Nagata, “Current status and prospects of lead-free piezoelectric ceramics,” *J. Eur. Ceram. Soc.*, vol. 25, no. 12, pp. 2693–2700, 2005.
[79] R. E. Eitel, C. A. Randall, T. R. Shrout, P. W. Rehrig, W. Hackenberger, and S.-E. Park, “New High Temperature Morphotropic Phase Boundary Piezoelectrics Based on $Bi(Me)O_3$–$PbTiO_3$ Ceramics,” *Jpn. J. Appl. Phys.*, vol. 40, no. 10R, p. 5999, Oct. 2001.
[80] H. Amorín, R. Jiménez, J. Ricote, T. Hungría, A. Castro, and M. Algueró,

"Apparent vanishing of ferroelectricity in nanostructured $BiScO_3$–$PbTiO_3$," *J. Phys. Appl. Phys.*, vol. 43, no. 28, p. 285401, Jul. 2010.

[81] T. Hungría, H. Amorín, M. Algueró, and A. Castro, "Nanostructured ceramics of $BiScO_3$–$PbTiO_3$ with tailored grain size by spark plasma sintering," *Scr. Mater.*, vol. 64, no. 1, pp. 97–100, Jan. 2011.

[82] M. Algueró, P. Ramos, R. Jiménez, H. Amorín, E. Vila, and A. Castro, "High temperature piezoelectric $BiScO_3$–$PbTiO_3$ synthesized by mechanochemical methods," *Acta Mater.*, vol. 60, no. 3, pp. 1174–1183, Feb. 2012.

[83] H. Amorín, R. Jiménez, M. Deluca, J. Ricote, T. Hungría, A. Castro, and M. Algueró, "Nanostructuring Effects in Piezoelectric $BiScO_3$–$PbTiO_3$ Ceramics," *J. Am. Ceram. Soc.*, pp. 1 – 8, May 2014.

[84] V. Porokhonskyy, S. Kamba, A. Pashkin, M. Savinov, J. Petzelt, R. E. Eitel, and C. A. Randall, "Broadband dielectric spectroscopy of $(1-x)BiScO_3$–$xPbTiO_3$ piezoelectrics," *Appl. Phys. Lett.*, vol. 83, no. 8, pp. 1605–1607, Aug. 2003.

[85] R. E. Eitel, C. A. Randall, T. R. Shrout, and S.-E. Park, "Preparation and Characterization of High Temperature Perovskite Ferroelectrics in the Solid-Solution $(1-x)BiScO_3$–$xPbTiO_3$," *Jpn. J. Appl. Phys.*, vol. 41, no. Part 1, No. 4A, pp. 2099–2104, 2002.

[86] M. T. Buscaglia, M. Viviani, V. Buscaglia, L. Mitoseriu, A. Testino, P. Nanni, Z. Zhao, M. Nygren, C. Harnagea, D. Piazza, and C. Galassi, "High dielectric constant and frozen macroscopic polarization in dense nanocrystalline $BaTiO_3$ ceramics," *Phys. Rev. B*, vol. 73, no. 6, p. 064114, Feb. 2006.

[87] M. H. Frey, Z. Xu, P. Han, and D. A. Payne, "The role of interfaces on an apparent grain size effect on the dielectric properties for ferroelectric barium titanate ceramics," *Ferroelectrics*, vol. 206, no. 1, pp. 337–353, 1998.

[88] A. V. Polotai, A. V. Ragulya, and C. A. Randall, "Preparation and Size Effect in Pure Nanocrystalline Barium Titanate Ceramics," *Ferroelectrics*, vol. 288, no. 1, pp. 93–102, 2003.

[89] G. Arlt, D. Hennings, and G. de With, "Dielectric properties of fine-grained barium titanate ceramics," *J. Appl. Phys.*, vol. 58, no. 4, pp. 1619–1625, Aug. 1985.

[90] G. Arlt, "Twinning in ferroelectric and ferroelastic ceramics: stress relief," *J. Mater. Sci.*, vol. 25, no. 6, pp. 2655–2666, Jun. 1990.

[91] D. Ghosh, A. Sakata, J. Carter, P. A. Thomas, H. Han, J. C. Nino, and J. L. Jones, "Domain Wall Displacement is the Origin of Superior Permittivity and Piezoelectricity in $BaTiO_3$ at Intermediate Grain Sizes," *Adv. Funct. Mater.*, vol. 24, no. 7, pp. 885–896, 2014.

[92] T. Hoshina, S. Wada, Y. Kuroiwa, and T. Tsurumi, "Composite structure and size effect of barium titanate nanoparticles," *Appl Phys Lett*, vol. 93, no. 19, p. 192914, 2008.

[93] J. M. Kiat, C. Bogicevic, P. Gemeiner, A. Al-Zein, F. Karolak, N. Guiblin, F. Porcher, B. Hehlen, L. Yedra, S. Estradé, F. Peiró, and R. Haumont, “Structural investigation of strontium titanate nanoparticles and the core-shell model,” *Phys Rev B*, vol. 87, no. 2, p. 024106, Jan. 2013.
[94] J. Petzelt, “Dielectric Grain-Size Effect in High-Permittivity Ceramics,” *Ferroelectrics*, vol. 400, no. 1, pp. 117–134, 2010.
[95] K. B. Lyons, P. A. Fleury, and D. Rytz, “Cluster Dynamics in a Dipolar Glass,” *Phys. Rev. Lett.*, vol. 57, no. 17, pp. 2207–2210, Oct. 1986.
[96] V. V. Laguta, M. D. Glinchuk, and I. V. Kondakova, “The Vogel-Fulcher law as a criterion for identifying a mixed ferroelectric-glass phase in potassium tantalate doped with lithium,” *Phys. Solid State*, vol. 46, no. 7, pp. 1262–1269, Jul. 2004.
[97] Y. N. Huang, X. Li, Y. Ding, Y. N. Wang, H. M. Shen, Z. F. Zhang, C. S. Fang, S. H. Zhuo, and P. C. W. Fung, “Domain freezing in potassium dihydrogen phosphate, triglycine sulfate, and CuAlZnNi,” *Phys. Rev. B*, vol. 55, no. 24, pp. 16159–16167, Jun. 1997.
[98] J. Bornarel, “Existence of Dislocations at Domain Tips in Ferroelectric Crystal KH_2PO_4,” *J. Appl. Phys.*, vol. 43, no. 3, pp. 845–852, 1972.
[99] M. Fally, A. Fuith, W. Schranz, and V. Müller, “Comment on ‘Origin of low-frequency dielectric dispersion in KH_2PO_4 and RbH_2PO_4 ferroelectric crystals,’” *Phys. Rev. B*, vol. 64, no. 2, p. 026101, Jun. 2001.
[100] V. Dorcet, P. Marchet, and G. Trolliard, “Structural and dielectric studies of the $Na_{0.5}Bi_{0.5}TiO_3$–$BiFeO_3$ system,” *J. Eur. Ceram. Soc.*, vol. 27, no. 13–15, pp. 4371–4374, 2007.
[101] C. Kruea-In, G. Rujijanagul, F. Y. Zhu, and S. J. Milne, “Relaxor behaviour of $K_{0.5}Bi_{0.5}TiO_3$-$BiScO_3$ ceramics,” *Appl Phys Lett*, vol. 100, no. 20, p. 202904, 2012.
[102] M. Kinka, M. Josse, E. Castel, S. Bagdzevicius, V. Samulionis, R. Grigalaitis, J. Banys, and M. Maglione, “Coexistence of ferroelectric and relaxor states in $Ba_2Pr_xNd_{1-x}FeNb_4O_{15}$,” *IEEE Trans. Ultrason. Ferroelectr. Freq. Control*, vol. 59, no. 9, pp. 1879–1882, 2012.
[103] M. Algueró, R. Jiménez, H. Amorín, E. Vila, and A. Castro, “Low temperature phenomena in ferroic $BiMO_3$–$PbTiO_3$ (M: Mn and Sc),” *Appl. Phys. Lett.*, vol. 98, no. 20, p. 202904, May 2011.
[104] H. Y. Guo, C. Lei, and Z.-G. Ye, “Re-entrant type relaxor behavior in $(1-x)BaTiO_3$–$xBiScO_3$ solid solution,” *Appl. Phys. Lett.*, vol. 92, no. 17, p. 172901, Apr. 2008.
[105] S. S. N. Bharadwaja, S. Trolier-McKinstry, L. E. Cross, and C. A. Randall, “Reentrant dipole glass properties in $(1 - x)BaTiO_3 - xBiScO_3$, $0.1 \leq x \leq 0.4$,” *Appl. Phys. Lett.*, vol. 100, no. 2, p. 022906, Jan. 2012.
[106] G. Xu, P. M. Gehring, and G. Shirane, “Coexistence and competition of local- and long-range polar orders in a ferroelectric relaxor,” *Phys. Rev. B*, vol. 74, no. 10, p. 104110, Sep. 2006.

[107] G. Arlt, U. Böttger, and S. Witte, “Dielectric dispersion of ferroelectric ceramics and single crystals at microwave frequencies,” *Ann. Phys.*, vol. 506, no. 7–8, pp. 578–588, 1994.
[108] T. Hoshina, Y. Kigoshi, S. Hatta, T. Teranishi, H. Takeda, and T. Tsurumi, “Size Effect and Domain-Wall Contribution of Barium Titanate Ceramics,” *Ferroelectrics*, vol. 402, no. 1, pp. 29–36, 2010.
[109] E. Buixaderas, V. Bovtun, M. Kempa, M. Savinov, D. Nuzhnyy, F. Kadlec, P. Vaněk, J. Petzelt, M. Eriksson, and Z. Shen, “Broadband dielectric response and grain-size effect in $K_{0.5}Na_{0.5}NbO_3$ ceramics,” *J. Appl. Phys.*, vol. 107, no. 1, p. 014111, Jan. 2010.
[110] G. Feuillard, V. Loyau, L. P. Tran-Huu-Hue, T. Wurlitzer, E. Ringgaard, W. Wolny, B. Malic, M. Kosec, A. Barzegar, D. Damjanovic, and M. Lethiecq, “Comparative performances of new KNN lead-free piezoelectric materials and classical lead-based ceramics for ultrasonic transducer applications,” in *2003 IEEE Symposium on Ultrasonics*, 2003, vol. 2, pp. 1995–1998 Vol.2.
[111] R. T. Brierley and P. B. Littlewood, “Domain wall fluctuations in ferroelectrics coupled to strain,” *Phys. Rev. B*, vol. 89, no. 18, p. 184104, May 2014.
[112] R. R. Newton, A. J. Ahearn, and K. G. McKay, “Observation of the Ferro-Electric Barkhausen Effect in Barium Titanate,” *Phys. Rev.*, vol. 75, no. 1, pp. 103–106, Jan. 1949.
[113] V. Porokhonskyy, L. Jin, and D. Damjanovic, “Separation of piezoelectric grain resonance and domain wall dispersion in $Pb(Zr,Ti)O_3$ ceramics,” *Appl. Phys. Lett.*, vol. 94, no. 21, p. 212906, May 2009.
[114] N. H. Asmar, *Partial differential equations with Fourier series and boundary value problems*. Pearson Prentice Hall, 2005.
[115] L. A. Santaló, *Integral Geometry and Geometric Probability*. Cambridge University Press, 2004.
[116] Y. Zhang, D. Xue, H. Wu, X. Ding, T. Lookman, and X. Ren, “Adaptive ferroelectric state at morphotropic phase boundary: Coexisting tetragonal and rhombohedral phases,” *Acta Mater.*, vol. 71, pp. 176–184, Jun. 2014.
[117] Y. Huan, X. Wang, Z. Shen, J. Kim, H. Zhou, and L. Li, “Nanodomains in KNN-Based Lead-Free Piezoelectric ceramics: Origin of Strong Piezoelectric Properties,” *J. Am. Ceram. Soc.*, vol. 97, no. 3, pp. 700–703, 2014.
[118] R. Theissmann, L. A. Schmitt, J. Kling, R. Schierholz, K. A. Schönau, H. Fuess, M. Knapp, H. Kungl, and M. J. Hoffmann, “Nanodomains in morphotropic lead zirconate titanate ceramics: On the origin of the strong piezoelectric effect,” *J. Appl. Phys.*, vol. 102, no. 2, p. 024111, Jul. 2007.
[119] N. A. Hill and A. Filippetti, “Why are there any magnetic ferroelectrics?,” *J. Magn. Magn. Mater.*, vol. 242–245, Part 2, no. 0, pp. 976 – 979, 2002.
[120] Y. Shimizu, Y. Fukuyama, T. Narikiyo, H. Arai, and T. Seiyama,

"Perovskite-Type Oxides Having Semiconductivity as Oxygen Sensors," *Chem. Lett.*, vol. 14, no. 3, pp. 377–380, 1985.
[121] B. Ostrick, M. Fleischer, U. Lampe, and H. Meixner, "Preparation of stoichiometric barium stannate thin films: Hall measurements and gas sensitivities," *Sens. Actuators B Chem.*, vol. 44, no. 1–3, pp. 601–606, Oct. 1997.
[122] H. Cheng and Z. Lu, "Synthesis and gas-sensing properties of $CaSnO_3$ microcubes," *Solid State Sci.*, vol. 10, no. 8, pp. 1042–1048, Aug. 2008.
[123] S. Upadhyay, O. Parkash, and D. Kumar, "Synthesis, structure and electrical behaviour of nickel-doped barium stannate," *J. Alloys Compd.*, vol. 432, no. 1–2, pp. 258–264, Apr. 2007.
[124] A. Aydi, S. Chkoundali, H. Khemakhem, A. Simon, and R. Von Der Mühll, "X-ray diffraction, dielectric measurements and Raman spectroscopy: Studies of the $(1 - x)CaSnO_3 - x\ NaNbO_3$ solid solution," *J. Alloys Compd.*, vol. 465, no. 1–2, pp. 222–226, Oct. 2008.
[125] V. Jayaraman, G. Mangamma, T. Gnanasekaran, and G. Periaswami, "Evaluation of $BaSnO_3$ and $Ba(Zr,Sn)O_3$ solid solutions as semiconductor sensor materials," *Solid State Ion.*, vol. 86–88, Part 2, pp. 1111–1114, Jul. 1996.
[126] B. Hadjarab, A. Bouguelia, A. Benchettara, and M. Trari, "The transport and photo electrochemical properties of La-doped stannate $BaSnO_3$," *J. Alloys Compd.*, vol. 461, no. 1–2, pp. 360–366, Aug. 2008.
[127] D. J. Singh, D. A. Papaconstantopoulos, J. P. Julien, and F. Cyrot-Lackmann, "Electronic structure of $Ba(Sn,Sb)O_3$: Absence of superconductivity," *Phys. Rev. B*, vol. 44, no. 17, pp. 9519–9523, Nov. 1991.
[128] J. Cerdà, J. Arbiol, R. Diaz, G. Dezanneau, and J. R. Morante, "Synthesis of perovskite-type $BaSnO_3$ particles obtained by a new simple wet chemical route based on a sol–gel process," *Mater. Lett.*, vol. 56, no. 3, pp. 131–136, Oct. 2002.
[129] A. S. Deepa, S. Vidya, P. C. Manu, S. Solomon, A. John, and J. K. Thomas, "Structural and optical characterization of $BaSnO_3$ nanopowder synthesized through a novel combustion technique," *J. Alloys Compd.*, vol. 509, no. 5, pp. 1830–1835, Feb. 2011.
[130] O. I. Prokopalo, "Conductivity and anomalous polarization in ceramicferroelectrics with perovskite structure," *Ferroelectrics*, vol. 14, no. 1, pp. 683–685, Jan. 1976.
[131] J. Cerdà, J. Arbiol, G. Dezanneau, R. Díaz, and J. R. Morante, "Perovskite-type $BaSnO_3$ powders for high temperature gas sensor applications," *Sens. Actuators B Chem.*, vol. 84, no. 1, pp. 21–25, Apr. 2002.
[132] A. Kumar, B. P. Singh, R. N. P. Choudhary, and A. K. Thakur, "A.C. Impedance analysis of the effect of dopant concentration on electrical properties of calcium modified $BaSnO_3$," *J. Alloys Compd.*, vol. 394, no.

1–2, pp. 292–302, May 2005.
[133] O. Parkash, D. Kumar, K. K. Srivastav, and R. K. Dwivedi, “Electrical conduction behaviour of cobalt substituted $BaSnO_3$,” *J. Mater. Sci.*, vol. 36, no. 24, pp. 5805–5810, Dec. 2001.
[134] W. Lu and H. Schmidt, “Lyothermal synthesis of nanocrystalline $BaSnO_3$ powders,” *Ceram. Int.*, vol. 34, no. 3, pp. 645–649, Apr. 2008.
[135] R. Köferstein, L. Jäger, M. Zenkner, and S. G. Ebbinghaus, “Nano-sized $BaSnO_3$ powder via a precursor route: Comparative study of sintering behaviour and mechanism of fine and coarse-grained powders,” *J. Eur. Ceram. Soc.*, vol. 29, no. 11, pp. 2317–2324, Aug. 2009.
[136] M. A. Green, K. Prassides, P. Day, and J. K. Stalick, “Structural properties of A_2SnO_4(A = Ba,Sr). A neutron diffraction study,” *J. Chem. Soc. Faraday Trans.*, vol. 92, no. 12, pp. 2155–2159, Jan. 1996.
[137] W. T. Fu, D. Visser, K. S. Knight, and D. J. W. IJdo, “Neutron powder diffraction study of phase transitions in Sr_2SnO_4,” *J. Solid State Chem.*, vol. 177, no. 11, pp. 4081–4086, Nov. 2004.
[138] A. Stanulis, S. Sakirzanovas, M. V. Bael, and A. Kareiva, “Sol–gel (combustion) synthesis and characterization of different alkaline earth metal (Ca, Sr, Ba) stannates,” *J. Sol-Gel Sci. Technol.*, vol. 64, no. 3, pp. 643–652, Dec. 2012.
[139] S. Omeiri, B. Hadjarab, A. Bouguelia, and M. Trari, “Electrical, optical and photoelectrochemical properties of $BaSnO_{3-\delta}$: Applications to hydrogen evolution,” *J. Alloys Compd.*, vol. 505, no. 2, pp. 592–597, Sep. 2010.
[140] H.-I. Yoo, C.-R. Song, and D.-K. Lee, “$BaTiO_{3-\delta}$: Defect Structure, Electrical Conductivity, Chemical Diffusivity, Thermoelectric Power, and Oxygen Nonstoichiometry,” *J. Electroceramics*, vol. 8, no. 1, pp. 5–36, Jul. 2002.
[141] A. Peláiz-Barranco, J. D. S. Guerra, R. López-Noda, and E. B. Araújo, “Ionized oxygen vacancy-related electrical conductivity in $(Pb_{1-x}La_x)(Zr_{0.90}Ti_{0.10})_{1-x/4}O_3$ ceramics,” *J. Phys. Appl. Phys.*, vol. 41, no. 21, p. 215503, Nov. 2008.